Deep-Sea Research, 1977, Vol. 24, pp. 511 to 548. Pergamon Press. Printed in Great Britain.

The chemistry, biology, and vertical flux of particulate matter from the upper 400 m of the equatorial Atlantic Ocean

JAMES K. B. BISHOP,*† JOHN M. EDMOND,† DARLENE R. KETTEN,†
MICHAEL P. BACON*‡ and WYATT B. SILKER§

(*Received* 1 *March* 1976; *in revised form* 2 *November* 1976; *accepted* 7 *November* 1976)

Abstract—Particulate matter, divided into <1, 1 to 53, and >53-μm size fractions, was obtained in profile from the upper 400 m at 2°47′N, 8°51′W in the equatorial Atlantic by large volume *in situ* filtration. The samples were analyzed for Na, K, Mg, Ca, carbonate, Si, Sr, Fe, C, N, P, organic $\delta^{13}C$, ^{7}Be, ^{214}Bi, ^{214}Pb, (^{226}Ra), ^{210}Po, and ^{210}Pb and were studied by light and scanning electron microscopy to determine the size and morphological distributions of the particles.

The chemical distributions in particulate matter are controlled largely by biological production, respiration, predation, aggregation, and fragmentation. The largest particulate elemental and mass concentration gradient occurs between 50 m (the base of the mixed layer, particle and organism maximum) and 113 m. The organic fraction was enriched with bound Mg and ion-exchangeable Ca and Sr. Dissolution of $SrSO_4$ from *Acantharia* Sp. was pronounced below 188 m. Large particles could be classified as crustacean appendage and carapace material, mucold material, hyaline or sheetlike material, fecal pellets, and fecal matter. The latter two types of fecal material, containing coccoliths, diatom fragments and other fine particles, become increasingly important with depth in the >53-μm size fraction with depth.

A model for particle settling constructed from the chemical and microscopic data indicates that 99% of the vertical mass *flux* through 388 m is carried by fecal matter and fecal pellets which contribute only 4% to the total suspended mass *concentration*. The sinking material has three major phases (flux in brackets): organic matter [94 mmoles $C\,cm^{-2}(1000\,yr)^{-1}$]; carbonate [10.9 mmoles $CaCO_3\,cm^{-2}(1000\,yr)^{-1}$]; and opal [12.1 mmoles $Si\,cm^{-2}(1000\,yr)^{-1}$]. Associated minor and trace components are transported vertically by a common mechanism but their regeneration depends on the chemistry of their carrier phases.

INTRODUCTION

THE CHEMISTRY and settling behavior of particulate matter is important in marine chemistry, geology, and biology. Most observed particulate matter has biological origin within the surface layer of the ocean. It sinks through the thermocline resulting in such phenomena as the familiar nutrient depletion of the surface layers and enrichment of the deep water column. The nutrient elements are largely recycled within the upper 1000 m of the water column; however, the complex nature of thermocline processes precludes the calculation of rates of recycling using dissolved nutrient data. Inefficiency in the recycling mechanisms operating in the water column allows the deposition of particulate matter. Bottom dwelling organisms metabolize most of the organic constituents, leaving

* Massachusetts Institute of Technology/Woods Hole Oceanographic Institution, Joint Program in Oceanography.

† Department of Earth and Planetary Sciences, Massachusetts Institute of Technology, Cambridge, Massachusetts 02139, U.S.A.

‡ Present address: United States Geological Survey, Denver, Colorado 80225, U.S.A.

§ Battelle, Pacific Northwest Laboratories, Richland, Washington 99352, U.S.A.

the mineral components to form the geological record of the oceanic conditions prevailing at the time of sediment deposition. Understanding the mechanisms important in the deposition of nannofossils (such as coccoliths) is important in paleo-oceanography. Determining the significant processes operating within the water column to change the character of the particulate matter will contribute to the knowledge of such basic processes as nutrient recycling and sediment formation.

The vertical flux of any chemical element in particulate matter depends on the size distribution, density, and settling behavior of the particles carrying that element. Ideally, one should determine the vertical chemical flux as a function of depth. Any changes in flux would be interpreted in terms of interaction of the particles with the water column. The flux of chemical elements to the bottom would give rates of material deposition. Towards these ends the Large Volume *in situ* Filtration System (LVFS) was constructed to collect samples of particulate matter amounting to several hundred milligrams dry weight from the upper 400 m of the water column in the open ocean.

BISHOP and EDMOND (1976) reported the preliminary results from particulate matter samples (split *in situ* into greater than and less than 53-μm size fractions) resulting from the filtration of up to 30 m^3 of seawater using the LVFS. They showed that particles smaller than 53 μm accounted for most of the mass concentration while the >53-μm particles carried 3 and 12 times the mass towards the sediments in areas of low and high biological productivity. These authors frequently found a particle maximum in the upper thermocline near the base of the mixed layer; in upwelling situations (southeast Atlantic) the mixed layer was poorly developed and the maximum particulate concentrations were nearest the sea surface. In this paper we wish to report the results from a variety of chemical and radiochemical analyses and from light and scanning electron microscopic studies of samples collected at LVFS Sta. 2 (2°47′N, 8°51′W, Dec. 19 to 20 1973, R. V. *Chain* 115-2 Dakar–Capetown). This station was typical of those exhibiting a particle maximum in the upper thermocline. By studying one profile in great detail we hope to provide a basis for understanding the important chemical, biological, and physical mechanisms operating to change the character of the particulate matter in the upper 400 m of the open ocean.

METHODS

BISHOP and EDMOND (1976) described the LVFS, its filters, and technique for filter handling prior to chemical analysis. Five to 30 m^3 of seawater were pumped *in situ* at a rate of about 6 $m^3 h^{-1}$ (maximum flow velocity 6 $cm s^{-1}$) through 53-μm Nitex mesh (25.4 cm effective diameter), and then through a pair of acid-leached precombusted Mead 935-BJ glass fiber (g-f) filters in series (each with pore size 1.25 μm at 98% efficiency, 0.8 μm at 75% efficiency; together they have a pore size of 0.8 μm at 96% efficiency at zero loading). The resulting sample was split into three size fractions: >53 μm, Nitex filter; 1 to 53 μm, top g-f filter; and <1 μm, bottom g-f filter.

The dry weight particulate matter concentrations for this station have already been reported (BISHOP and EDMOND, 1976). All chemical analyses were of subsamples of the filters, either by weight or by area fraction. Subsampling by area was both faster and more accurate; specially machined and polished brass cork borers were used to sample the g-f filters. A scalpel and a glass template were used to subsample the Nitex prefilters. The accuracy of the chemical analyses, of the blank corrections, and of the subsampling procedure was established by replicate analyses.

Major constituents

Na, K, Mg, Ca, and Sr were determined by leaching the filter subsamples [1/80 and 1/40 of each glass fiber (g-f) filter and Nitex prefilter, respectively] in 0.6 N HCl for 24 h or in 2.2 M acetic acid for 70 h. K was not measured in g-f samples as blank levels were too high (4 mg). The leach solutions were filtered (0.6-μm Nuclepore filter), made up to 50 ml, and analyzed by flame atomic absorption (Perkin–Elmer Model 403). Samples, standards, and blanks were treated identically.

Na, Mg, K, and Ca in the acid-leach solutions had three sources: filter blank, sea salt, and particulate matter.

Table 1. Major ion blank levels* in Mead 935-BJ glass fiber filters.

Sample description	n†	Na/ σ_{Na}	Mg/ σ_{Mg}	Ca/ σ_{Ca}
Untreated Mead 935-BJ	(1)	37. / -	2.7 / -	4.8 / -
JB - 91 unused blank L.V.F.S. Stn. 2	(4)	10.0 /1.56	0.697/0.073	2.74/0.059
JB - 91 Rockport blanks	(5)	5.00/0.46	0.586/0.066	2.27/0.23
JB - 108 Rockport blank (Batch 9)	(4)	5.75/0.77	0.603/0.068	2.79/0.27
JB - 121 Rockport blank (Batch 9)	(4)	6.46/0.95	0.823/0.065	3.77/0.49
All Rockport blank filters	(16)	5.63/0.85	0.632/0.107	2.62/0.66
L.V.F.S. Stn. 2** bottom filters (388m data omitted ?)	(5)	5.00assumed	0.654/0.153	2.78/0.79

* Acid leachable blanks (0.6 N HCl), results are in milligrams per 25.4 cm diameter g-f filter.

** The Na analyses of these filters were corrected assuming a 5-mg Na blank (JB-91 Rockport blank). The residual Na was assumed to be due to sea salt and was used to correct the Mg and Ca analyses of these filters resulting in the filter blank estimate for both Ca and Mg.

† n = number of subsamples analyzed.

The appreciable Na, Mg, and Ca blank levels in the untreated glass fiber filters (Table 1, line 1) were reduced by leaching batches of 15 to 20 filters with 300 to 500 ml of concentrated HCl for 12 h and then washing them with doubly distilled deionized water until neutral pH was measured in the effluent. The filters were then dried for 24 h at 100°C and combusted, separated by Pyrex glass rods, at 450°C for 2.5 h. The top and bottom filters from the stack were discarded; the others were weighed and placed in numbered polyethylene bags in the same order as they were in the stack. Consequently, the top and bottom g-f filters for each LVFS sample were next to each other throughout their whole history, from pretreatment to analysis. Generally, one batch of filters was used at each station with one filter being reserved for blank determinations.

To determine if the unused blank filters were true blanks for those filters used in the LVFS (exposed to seawater and distilled water washed), 47-mm diameter subsamples of unused blank filters from different batches were dipped in surface seawater at Rockport, Massachusetts, for periods up to 3 h. They were then treated in exactly the same fashion as the LVFS filters. Subsamples were leached with 0.6 N HCl to determine the Na, Ca, and Mg blank values and also were analyzed for C and N to investigate the possibility of adsorption of these elements from seawater onto the glass filters. Compared to unused JB-91 (LVFS Sta. 2 blank; Table 1, line 2) the subsamples of this blank filter, after exposure to Rockport seawater and treatment as the other LVFS samples, had lower and more reproducible acid-leachable sodium content (Table 1, line 3). This was true for all batches

and so the 'Rockport' blanks were considered better than unused blanks for the correction of the LVFS data.

Replicate analyses of the Rockport blank filters indicated that individual filters had more uniform blank levels than all filters (Table 1, lines 3 to 6). Rockport blank filters JB-108 and JB-121 were the top and bottom filters of one batch and had different blank levels. The use of one blank to correct the analyses of filters from its batch results in a 0.7-mg maximum uncertainty for Na, 0.22 mg for Mg, and 1.0 mg for Ca.

Since the top and bottom glass fiber filters for each LVFS sample were next to each other in their batch they are assumed to have similar blank levels. Each sodium analysis was corrected by subtracting 5.0 mg (JB-91, Rockport) and the remaining Na was assumed to be from sea salt (BISHOP and EDMOND, 1976). The Mg and Ca analyses of each bottom filter were corrected for sea salt and the residuals were subtracted from the analyses of the corresponding top filter. Blank values for Mg and Ca so calculated were comparable to the Rockport blank values (Table 1). The Sr analyses were corrected in the same way (typical blank = 0.01 mg). Major-ion blanks of the Nitex mesh were an order of magnitude lower and presented little problem when correcting the analyses of the prefilters.

Carbon and nitrogen were determined directly on subsamples of the g-f filters (1/80th of the filter, Perkin–Elmer Model 240 CHN analyser; CULMO, 1969). Because Nitex mesh (> 53 μm fraction) has a C/N ratio of about 6, particles were removed before analysis using a stiff nylon brush and sucked onto a pre-weighed, precombusted Whatman GFF filter in a 13-mm in-line Millipore® filter holder. The procedure was monitored at 12× on a Wild M5 Stereomicroscope. After examination at 50×, Nitex fibers were removed, and the filters were reweighed (Perkin–Elmer Model AD-2 autobalance). Particle recovery was calculated as the product of the mass of particles recovered and the area factor divided by the total dry weight of particles on the Nitex filter; it was approximately 50%. Bias introduced by this technique is probably small but would favor the larger particles. Carbonate was removed before analysis by exposing the subsamples to fuming HCl in a closed container for 24 h and then drying at 60°C for 8 h.

The C and N analyses of JB-91 (Table 2) showed *lower* levels of C and similar levels of N compared to subsamples of the unused blank filter; in addition there was no evidence of uptake of C or N by the g-f filters from the surface seawater with time (Table 2). Analyses of C and N were therefore corrected using Rockport JB-91 as blank (questionable N data omitted).

$\delta^{13}C$ in the organic material was determined by the method of DEGENS (1969). Before analysis, the subsamples of the g-f filters and the particles removed from the Nitex were

Table 2. Carbon* and nitrogen uptake by Mead 935-BJ glass fiber filter from 'Rockport' seawater.

Sample	C	N	Hours:Min Exposure Time
JB-91 Unused	4.94	0.27	0:00
" "	5.02	1.07 (?)	0:00
JB-91 Rockport	2.64	0.23	0:01
JB-91 Rockport	2.22	0.22	0:30
JB-91 Rockport	2.26	0.31	1:22
JB-91 Rockport	1.76	0.60 (?)	2:52
Avg. Rockport	2.22 ± .36	0.25 ± .05	

* Milligrams of carbon and nitrogen per 25.4 cm diameter g-f filter.

Table 3. Chemical data *Chain* 115-2 LVFS Sta. 2. Upper: > 53-μm size fraction analyses. Lower: < 53-μm size fraction analyses.

z (m)		Na (mg)	xs Mg (mg)	xs K (mg)	Ca (mg)	Sr (mg)	C_{inorg} (mg)	Si (mg)	Fe (mg)	C_{org} (mg)	N (mg)	P (mg)	$\delta^{13}C_{PDB}$ (‰)	mass (gm)	vol. (m^3)	weight (10^3kg)
32	a	3.59	0.13	0.13	1.39		a 0.357 d 0.788	f 0.344		15.2	2.25	0.239	-23.16	0.042	4.57	4.67
	a						a 0.408 e 0.889			15.7	(3.77)	0.145			±.15	
	b	4.36	0.12		1.55	0.276										
	c	2.81	0.148	0.10	1.83	0.276										
50	a	0.90	0.242	0.09	2.11		a 0.511 d 3.17	f 0.271		36.4	lost	0.512	-22.72	0.105	4.47	4.58
	a	2.01	0.264	0.15	2.26		a 0.594 e 3.25			36.7	5.17	0.680			±.15	
	b	1.87	0.25		2.24	0.419										
	c	1.53	0.236	0.15	2.42	0.483										
113	a	1.05	0.130	0.02	4.01		a 1.181 d 3.861	f 0.320		17.8	2.04	0.151	-23.32	0.070	12.79	13.13
	a						a >.9 e 3.69			19.1	2.23	0.180			±.3	
	b	0.36	0.12		3.78	0.122										
	c	0.61	0.201	0.01	4.37	0.160										
188	a	1.17	0.143	0.01	2.99		a 0.887 d 2.88	f 0.337		14.0	1.68	0.097	-23.62	0.060	17.82	18.30
	a	1.27	0.137	0.02	3.06		a 0.942 e 4.15			14.3	1.70	0.104			±.4	
	b	1.48	0.19		3.60	0.158										
	c	2.43	0.189	0.00	3.28	0.093										
294	a	1.03	0.198	0.01	3.63		a 1.076 d 3.03	f 0.473		12.5	1.58	0.056	-23.30	0.063	21.14	21.71
	a	2.15	0.238	0.08	4.44		a 1.357 e 3.10			15.9	1.97	0.094			±.6	
	b	1.00	0.14		4.27	0.100										
	c	0.82	0.196	0.02	2.12	0.061										
388	a	0.57	0.157	-.01	3.10		a 0.910 d 2.42	f 0.489		4.64	0.549	0.049	-23.72	0.019	23.70	24.34
	a	0.49	0.163	-.02	2.76		a 0.834 e 3.05					0.061			±.6	
	b	1.66	0.15		3.22	0.097										
	c	1.02	0.153	0.03	4.04	0.087										
BLANK		0.34	0.058	0.07	0.105	0.001	0.0007	0.05	0.040	0.4	0.031	0.014		.026		

32	b	11.2	0.03		2.62	0.144	a 0.82	fT 0.99	T 32.9	4.83	0.476/.026	-19.95	0.128	4.57	4.67
	c	12.6	0.53		2.39	0.101	a 0.73						0.159	±.15	
								fB 0.44	B 9.1	1.45	0.155/.011	-21.98			
50	b	14.0	0.17		3.47	0.128	a 0.87	fT 0.52	T 37.6	5.40	0.639/.107	-23.05	0.140	4.47	4.58
	c	13.8	0.44		3.19	0.115			T 38.3	5.39		-24.12	0.174	±.15	
								fB 0.53	B 12.8	2.14	0.239/.069	-26.41			
							a 8.06								
113	b	6.34	0.69		30.80	0.448	a 8.04	fT 1.36	T 50.6	5.89	0.454/.015	-23.25	0.208	12.79	13.13
	c	6.31	0.68		27.69	0.468	a 7.88	fT 1.30	T			-22.69	0.217	±.3	
							a 7.84	fB 0.63	B 10.0	1.67	0.135/.025	-23.10			
							a 7.85	fB 0.64							
188	b	16.0	0.75		29.03	0.362	a 7.79	fT 2.00	T 56.9	6.20	0.495/.008	-22.27	0.234	17.82	18.30
	b	14.0	0.60		25.26	0.342	a 7.86		T 56.7	5.95		-21.65	0.232	±.4	
	c	14.3	1.13		27.52	0.345		fB 0.36	B 9.8	1.22	0.096/.003	-21.06	0.222		
294	b	10.62	2.31		37.03	0.351	a 9.22	fT 3.88	T 63.3	6.62	0.527/.006	-20.79	0.285	21.14	21.71
	c	7.02	1.46		33.27	0.370	a 9.03	fT 4.22	T 59.6	6.08			0.273	±.6	
								fB 0.54	B 8.8	0.82	0.166/.006	-21.05			
								fB 0.54	B 8.8	0.81					
388	b	73.9	0.70		31.48	0.248	a 8.90	fT 4.53	T 57.6	5.66	0.525/.010	-20.98	0.368	23.70	24.34
	b	85.5	0.90		31.98	0.225	a 8.91						0.330	±.6	
	c	38.6	-.86		33.38	0.226		fB 0.64	B 14.3	2.81	0.220/.002	-21.13	0.541		
BLANK		5.0 ±.7	0.58		2.5	0.01	0.12 ±.03		1.10 ±.01	2.2 ±.7	0.24 ±.11	0.006	-21.53	0.000 ±.013		

a: 20% H_3PO_4; b: 2.0 M HAc; c: 0.6 N HCl; d: 1 N NaOH; e: 0.4 M Na_2CO_3; f: 0.6 N HCl, 0.2 M $NH_2OH \cdot HCl$; T: Top glass fiber filter = 1- to 53-μm size fraction; B: Bottom glass fiber filter = < 1-μm size fraction; mass: particulate dry weight = < 1 μm + 1- to 53-μm size fractions according to BISHOP and EDMOND (1976).

flooded with 6 N HCl in precombusted ceramic boats and taken to dryness (70°C) three times to remove carbonate.

Particulate carbonate was determined in a closed recirculation system using a Beckman 215 i.r. analyzer and calcite standards (MENZEL and VACCARO, 1964). Carbon dioxide was generated using 20% phosphoric acid in a Y-tube (CRAIG, 1953). The residual phosphoric acid solutions from the > 53-μm fraction were retained for analysis of Na, K, Mg, and Ca.

Particulate Fe was determined by autoclaving subsamples of the filters in the presence of 0.2 M hydroxylamine hydrochloride and 0.6 N hydrochloric acid for 18 h. The resulting solution was filtered and analyzed using the method of STOOKEY (1970). The blank values

for g-f filters were significant (1.12 mg), accounting for 50% of the measured iron in some samples, but replicate blanks agreed within 1%.

Phosphate was released from the particles by repeated treatment with saturated potassium persulphate solution followed by autoclaving for 30 min (three times). The particles were completely bleached by this treatment and the Nitex virtually destroyed. The samples, standards, and blanks were processed identically, filtered and analyzed following MURPHY and RILEY (1962). The rate of color development was lower than for normal seawater, stabilizing only after 6 h.

It was not practical to analyze the material on the g-f filters for silica. However, samples had been collected from 30 l. Niskin samplers on 0.4-μm Nuclepore filters for intercalibration (BISHOP and EDMOND, 1976). These were digested at 120°C in 10 N NaOH for 2 h in Teflon beakers. After neutralization with 6 N HCl the granular precipitate was removed by filtration and the sample analyzed following MULLIN and RILEY (1955). Standards were treated identically; no interference from the Nuclepore filters was found. Silica was leached from the $\gtrsim$53 μm samples using either 0.4 M Na_2CO_3 or 1 N NaOH solutions at 60°C for 24 h. After filtration and neutralization with HCl the solutions were analysed as above.

Table 3 lists the analytical results and filter blanks for the various elements discussed above. For purposes of material balance in the particulate matter, the results are tabulated in milligrams of element per sample. Chemical units (nanomoles per kilogram) are used in discussions of elemental relationships and distributions and in calculations of vertical fluxes of particles in the water column.

Radioisotopes

One-half of each of the filters was analyzed non-destructively by gamma-ray spectroscopy for the cosmic ray produced isotope ^{7}Be ($t_{1/2}$ = 53 days) and the ^{226}Ra daughters ^{214}Bi and ^{214}Pb using a Ge(Li) detector.

1/90 to 1/30 of each filter sample was analyzed for ^{210}Pb and ^{210}Po activity according to the method of BACON (1975). The only modification of the analytical procedure was the use of HF to destroy the g-f filter.

Microscopy

The samples of particulate matter on either g-f filter or Nitex mesh were prepared for scanning electron microscopy (SEM) by standard procedure, coating them with carbon and gold. Routine examination of the samples was made at 2500 × using a Japan Electron Optics Laboratory (JEOL) Model J.S.M.-U3 scanning electron microscope.

For light microscopy, the 1 to 53-μm (g-f) filter samples (0.92 cm diameter) were placed on a glass slide, wetted with Cargille's Type B Immersion Oil (n_d^{25} = 1.5150), degassed in a vacuum desiccator for several hours and permanently affixed with a No. 1 cover slip and sealed with silicone rubber cement. Preparation of the > 53-μm samples involved the use of saturated phenol–toluene solution washes to dissolve the Nitex mesh and deposit the particles onto a Whatman GFF g-f filter. The filter was then rinsed with toluene to remove the phenol and dried at 60°C on a hot plate for 30 min. The removal of the Nitex grid was necessary as this material is strongly birefringent under polarized light and masks the presence of some organisms. Mounting of the samples onto glass slides followed the procedure outlined above.

The slides were examined at magnifications of 150 to 800× on a phase-contrast Olympus POM microscope and at magnifications of 50 to 200× on a Wild M-5 Stereomicroscope to determine the depth distributions of organisms and large aggregate particles. Identifications were completed to genera whenever possible. When this was not possible, organisms were listed by order or by similar appropriate classifications; i.e. Coccolithophoridae; Foraminiferida; centrate, pennate, solenoid, or gonioid diatoms; Radiolaria; Acantharia; gymnodinial or peridinial dinoflagellates; and such macroinvertebrate structures as poriferan spicules and portions of crustacean carapaces and appendages. The more general designations were considered sufficient for the context of this paper as they included most organisms encountered and adequately distinguished their chemical composition. Values for the concentration of organisms at each depth are therefore computed on the basis of these classifications.

RESULTS AND DISCUSSION

A hydrographic profile was made to 550 m (Fig. 1) to provide an oceanographic context for the LVFS samples and as an aid in choosing sampling depths. There was a 40-m mixed layer with the salinity maximum of the sub-tropical underwater at 46 m. The TS relation between 50 and 500 m falls in the field of South Atlantic Central Water. There is

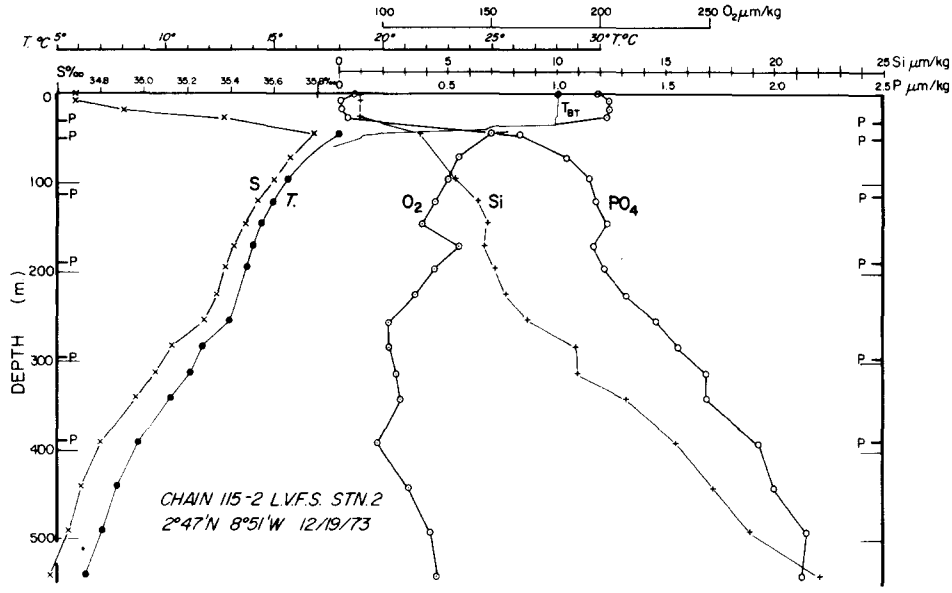

Fig. 1. Hydrography of upper 500 m at *Chain* 115-2 LVFS Sta. 2. LVFS depths are indicated by the letter P.

a maximum in oxygen and minimum in phosphate in the mixed layer and sharp vertical gradients in the thermocline. Below 200 m the phosphate and silicate increase regularly with depth; the oxygen concentrations are quite uniform. During the station the ship drifted 25 km to the northeast at an average of 30 cm s^{-1} although the winds were light. A 12 kHz Precision Graphic Recorder was used to monitor the depth of the LVFS as well as to observe the vertical migration of the deep scattering layer during the station (Fig. 2).

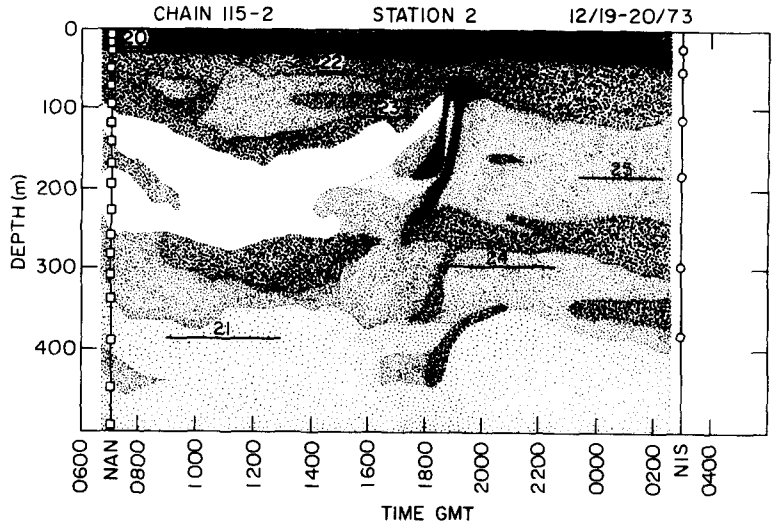

Fig. 2. Graphic reproduction of 12-kHz Precision Graphic Recorder record obtained at the station. Shading is proportional to back-scattering of sound by the deep-scattering layer organisms. LVFS, Nansen, and 30-l. Niskin sample depths and times are shown. Time zone −1.

Gravimetric results

The weights of suspended material on the filters calculated using the analytical data (taking organic carbon as CH_2O) agree well with the measured values (Table 4, Fig. 3) save for the deepest and two shallowest < 53-μm LVFS samples. The replicate sodium analyses on the deep sample were poor and hence the computed gravimetric weight has a high uncertainty. It is possible that there is an appreciable contribution of non-biogenic material to the surface weights although this has not been verified directly.

Table 4. Particulate mass concentration.

Depth	Chemical* dry weight concentration	Gravimetric dry weight concentration	$\sigma_{Grav.}$
(m)	(μg kg^{-1})	(μg kg^{-1})	(μg kg^{-1})
32	10.26	9.0	5.6
50	24.67	22.9	5.7
113	5.24	5.3	2.0
188	2.99	3.3	1.4
294	2.58	2.9	1.2
388	1.12	0.9	1.1
32	26.25	30.7	5.6
50	31.55	35.1	6.1
113	17.54	16.2	0.4
188	12.96	12.5	0.9
294	12.54	12.9	0.8
388	10.68	17.0	4.7

*Calculated as $CH_2O + N + PO_4 + CaCO_3 + SiO_2 + SrSO_4$ + excess Ca + excess Mg + excess K + Sr (in $CaCO_3$).

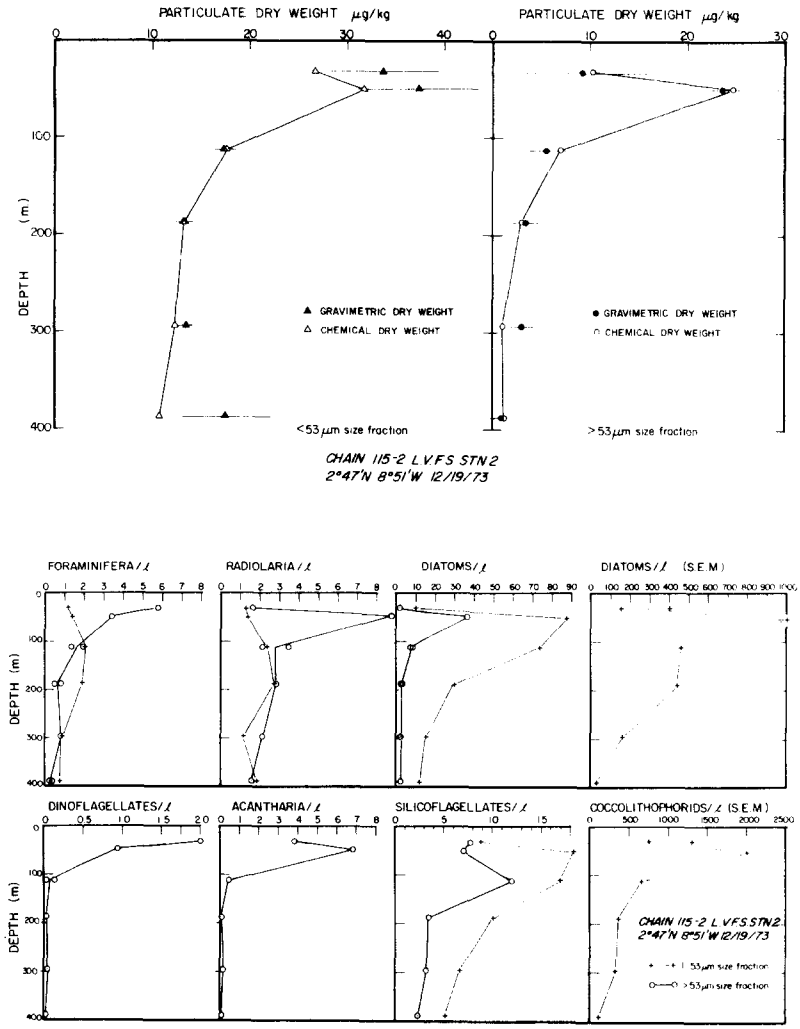

Fig. 3. Upper: particulate dry weight profiles of < 53- and > 53-μm size fractions. Open symbols are computed from the sum of $CH_2O + N + P + CaCO_3 + SiO_2 + SrSO_4$ + excess Ca + excess Mg + K + Sr (in $CaCO_3$); closed symbols are total dry weight measurements. Comparison of the two sets of data shows that most particles in the upper 400 m are biogenic. Lower: plankton distributions showing maxima at the depth of the particle maximum. Abundances shown are much higher than previously reported (e.g. Foraminifera) but are typical of other LVFS stations. This is primarily because the LVFS acts like a 1-μm plankton net and catches organisms usually missed in plankton tows. Two points indicate counts of different subsamples of the same filter.

Biological observations

Both the large and small size fractions exhibit a dry weight concentration maximum at 50 m, just below the base of the mixed layer in the upper thermocline. Microscopic examination of the filters showed that many phytoplanktonic and microzooplanktonic organisms have maximum population densities at this depth.

The most abundant organisms in the > 53-μm size fraction are Foraminifera,

Table 5. Plankton abundances at *Chain* 115-2 LVFS Sta. 2. Upper: >53-μm size fraction (whole tests m^{-3}). Lower: 1- to 53-μm size fraction (whole tests m^{-3}).

z	Foraminifera (LM)	Radiolaria[a] (LM)	Diatoms (LM)	Silico-flagellates (LM)	Acantharia (LM)	Dino-flagellates (LM)	Cocco-lithophoridae (SEM)	Diatoms (SEM)
32	5780	1605/	140	7775	3815	2000		
50	3760	8690/	35900	6810	6810	940		
113	1350		8840			14		
	1970	4690/3500	7250	11950	426	137		
188	470		2010			15		
	805	3780/2855	3060	3420	73	42		
294	800	2640/	2250			37		
	805	2840/2130	2550	3205	180	0		
388	232					5		
	383	2720/1575	2210	2350	84	0		
32	1160	1275	9970	8800	0		1.30 x 10^6	0.15 x 10^6
							0.75 x 10^6	0.40 x 10^6
50	1360	1360	87280	18340	0		2.03 x 10^6	1.03 x 10^6
113	2015	2370	73770	16960	0		0.65 x 10^6	0.46 x 10^6
188	1875	2730	29850	10060	0		0.36 x 10^6	0.44 x 10^6
294	863	1150	15610	6620	0		0.33 x 10^6	0.16 x 10^6
388	769	1860	12040	5120	0		0.11 x 10^6	0.03 x 10^6

a. Radiolarian counts are broken down as: total whole tests (including juveniles)/adult forms.
b. Replicate counts are indicated.
c. LM light microscopy; SEM scanning electron microscopy.

Radiolaria, diatoms, and Acantharia (Table 5, Fig. 3). The density of 3 to 6 Foraminifera per liter of near-surface waters is much higher than previously reported values of approximately 10 m^{-3} (BERGER, 1968; BOTTAZZI, SCHREIBER and BOWEN, 1971) obtained from 250-μm mesh plankton net tows in the tropical Atlantic. Foraminifera in the >53-μm fraction ranged in size from 20 to approximately 200 μm; they averaged 20 μm in the <53-μm fraction. Our foraminiferan counts at this station are representative of those obtained at other LVFS stations and so the increased number of Foraminifera sampled by the LVFS can only be explained by the difference in its filtration efficiency from that of plankton nets. Counts of Foraminifera larger than 100 μm are comparable to values obtained from plankton tows.

The Foraminifera, primarily belonging to the Globigerinidae, reach their maximum density at 32 m. At this depth they are largely single prolucula or megalospheric individuals in the early stages of division. Light microscopy of the samples showed that approximately 80% of the foraminiferal tests were occupied (cytoplasm present) at 32 and 50 m and SEM examination of similar forms showed them to be associated with organic material (Fig. 4; A, B). These organisms appear to have been alive at the time of sampling. Below 50 m only 10 to 20% of the tests were occupied. SEM showed the empty tests to be completely devoid of organic material (Fig. 4, E) and essentially 'clean'. It was also observed that below 100 m the 'live' Foraminifera were generally multichambered, microspheric forms seldom seen in the shallower samples and that the larger, megalospheric tests were completely empty. This apparent distribution indicates that alternating sexual (microspheric) and asexual (megalospheric) generations may occur at different depths, but this needs further investigation. A detailed study of the Foraminifera is underway.

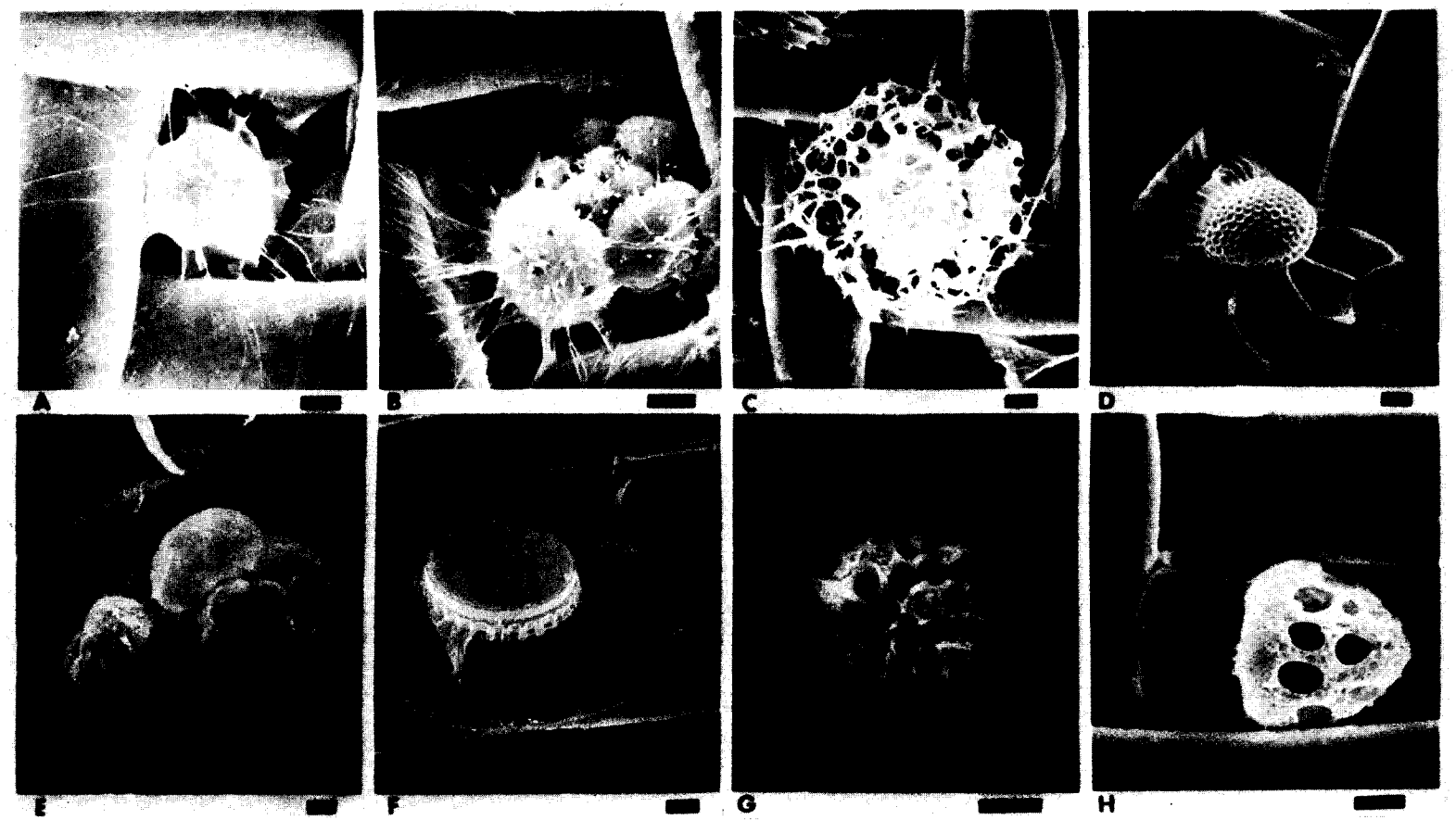

Fig. 4. Scanning electron micrographs of plankton sampled by LVFS. Scale is indicated in each photo: bars indicate 10 μm. Grid visible is 53-μm Nitex. A. Foraminifera, fam. Rotaliidae with pseudopodia, 32 m. B. Foraminifera, *Hastigerina* sp. Note reticulopods with associated organic material, 32 m. C. Radiolaria with intact inner capsule, 32 m. D. Peridinial dinoflagellate, *Ornithocercus* sp., 32 m. E. Foraminifera of the family Globigerinidae, 113 m. F. *Planktoniella* sp., a centrate diatom with a membranous, hyaline extension of extracellular loculi, 50 m. G. Radiolaria of the genus *Hexalonche*, family Sphaeroidae, 188 m. H. Tintinnid, *Codonellopsis* sp., with fenestrated lorica. Lower margin of lorica is composed of coccoliths, 32 m.

(facing p. 520)

Dinoflagellates (Fig. 4D) also show a maximum population at 32 m and are essentially absent from the > 53-μm fraction below 50 m. This is an indication of the friability of these organisms compared with the Foraminifera.

Radiolaria, diatoms, and Acantharia show maximum population densities at 50 m in the > 53-μm fraction. Apart from the 50-m maximum, the Radiolaria (e.g. Fig. 4C and G) show little species and developmental variability throughout the water column except for the large number of initial spicules or early developmental stages near 300 m. The diatom population in the > 53-μm fraction is dominated by coscinodiscoid species (e.g. Fig. 4F) and by *Rhizosolenia* sp. Below 150 m, the diatom frustrules are generally empty and many are fragmented. Their presence and condition is probably a result of predation at shallower depths. Light microscope examination of the < 53-μm fraction revealed a diatom maximum also at 50 m; SEM showed a diatom population approximately ten times that determined by light microscopy and revealed many forms, particularly pennate diatoms, that were too small (i.e. < 10 μm) to be seen easily by light microscopy at 400 ×. The Acantharia consist primarily of Acanthometridae at the shallower depths; however, it is difficult to classify these organisms below 100 m because of loss of major spines and dissolution of fine structures (see below).

Tintinnids (e.g. Fig. 4D) are relatively rare, having population densities between 1000 m^{-3} near the surface and 20 to 30 m^{-3} below 200 m.

Silicoflagellates occur predominantly in the < 53-μm fraction with a maximum at 50 m; the population is essentially uniform, showing little variation in species or developmental stages.

SEM examination showed the coccosphere distribution to reach a maximum of two individuals per ml at 50 m. Below 50 m, the < 53-μm fraction is dominated by coccoliths and diatom fragments, and at 388 m only the smallest coccospheres (5 to 10 μm) survive intact; the larger forms are all fragmented.

The particle maximum coincides with the maxima in the organisms. Primary producers (and their predators) occupy the upper thermocline in areas where it and the euphotic zone overlap. There, autotrophs take advantage of the increased levels of nutrients with some sacrifice of solar energy. The sudden change in condition and numbers of the whole organisms between 50 and 113 m must be due to primary and secondary level predation.

Organic C, N, P, *and* ^{13}C

The three filters from each depth were analyzed; these correspond to the < 1-μm (bottom g-f), 1- to 53-μm (top g-f), and > 53-μm (Nitex) fractions (Table 6). The total carbon values for the < 1-μm fraction were not corrected for carbonate (the correction would be < 2‰); those for the 1- to 53-μm fraction were corrected using the carbonate-carbon data. The carbonate was removed from the > 53-μm fraction by HCl fumes before analysis. While they are low it is assumed that the carbon values measured on the bottom g-f filter are particulate because adsorption of dissolved carbon was ruled out by experiment (Table 2). It is unlikely that washing of the fresh filter with distilled water caused preferential loss of phosphorus or nitrogen relative to carbon. Comparison of C/P and C/N ratios in the 1- to 53-μm fraction with those from Sta. 1 (12°06'N, 17°43'W), where the filters were not washed, indicates no systematic effects attributable to washing. In the absence of direct experiments, material loss due to washing is indeterminate and is assumed to be small.

Table 6. Particulate C_{org}, N. P. $\delta^{13}C$ data (nmoles kg^{-1}).

		>53μm SIZE FRACTION										
z (m)	δC^{13}_{PDB} (‰)	C_{org}	$\sigma_{C_{org}}$ †	C^*_{org} ††	N	σ_N †	N* ††	P	σ_P †††	C_o/N	C_o/P	% organic †*
		(n moles / kg)								(mole ratio)		
32	-23.16	271 280	168 173	> 49 > 53	34.4 (56.2?)	13.8 -	> 6.19 -	1.33	0.33	7.9 (5?)	204	99 (103)
50	-22.72	662 667	165 167	>152.3 >120.1	- 80.7	- 20.2	- >14.5	4.20	0.59	- 8.3	158	(91) 93
113	-23.32	113 121	41 44	> 52 > 53	11.1 12.1	4.00 4.36	> 5.11 > 5.32	0.408	0.037	10.2 10.0	285	67 69
188	-23.62	63.7 65.1	28 29	> 27 > 27	6.56 6.64	2.89 2.92	> 2.82 > 2.72	0.178	0.005	9.7 9.8	361	61 66
294	-23.30	47.9 61.0	19 24	> 20 > 19	5.20 6.48	2.08 2.59	> 2.18 > 2.01	0.111	0.029	9.2 9.4	490	52 66
388	-23.72	15.9	22	> 12.2	1.61	2.25	>1.24	0.073	0.008	9.8	218	64

	< 1 μm SIZE FRACTION						1 - 53 μm SIZE FRACTION						
z (m)	δC^{13}_{PDB} (‰)	ΣC**	N	P	σ_P	C/N	C/P	δC^{13}_{PDB} (‰)	C_{org}	N	P	σ_P	C/N	C/P
		(n moles / kg)				mole ratio			(n moles/kg)				mole ratio	
32	-21.98	161	22.2	1.07	0.08	7.3	151±7	-19.95	571	73.8	3.29	.18	7.74	174±4
50	-26.41	234	33.4	1.68	0.49	7.0	139±24	-24.12 -23.05	670 683	84.3 84.1	4.50	.76	7.96 8.12	149±20 151±20
113	-23.10	63.2	9.1	.33	0.06	6.95	190±22	-22.69 -23.25	268	32.0	1.12	.03	8.38	240±7
188	-21.06	44.4	4.76	.169	0.006	9.3	263±5	-22.27 -21.65	222 221	24.2 23.2	.873	.014	9.17 9.51	254±4 253±4
294	-21.05	33.6 33.6	2.70 2.67	.247	0.009	12.4 12.6	137±3	-20.79	208 194	21.8 20.0	.783	.009	9.55 9.69	265±2 247±2
388	-21.13	48.9	8.25	.292	0.002	5.9	167±1	-20.98	164	16.6	.696	.013	9.86	235±3

† Error due to estimate of recovery from dry weight data.

†† Analytical value indicates minimum amount of carbon and nitrogen on the prefilter C^*_{org}/C_{org} = recovery of particles.

†* % organic component as $(CH_2O + N)/\Sigma$ dry weight of particles removed from the Nitex mesh.

††† Standard deviation of 2 analyses.

** Carbonate contribution to ΣC is less than 2%.

All three size fractions display pronounced maxima in the organic carbon, nitrogen, and phosphorus concentrations at 50 m coincident with the observed maximum population of plankton (Fig. 5). The largest change in concentration of these elements was between 50 and 113 m. The largest gradient is in the > 53-μm fraction and the smallest in the < 1-μm fraction, indicating perhaps that filter-feeding organisms utilize the largest particles preferentially. Below 113 m the carbon, nitrogen, and phosphorus concentrations decrease slowly with depth. The C/N and C/P ratios of the particles are a function of both size and depth, being lowest in the < 1-μm fraction and highest in the > 53-μm fraction.

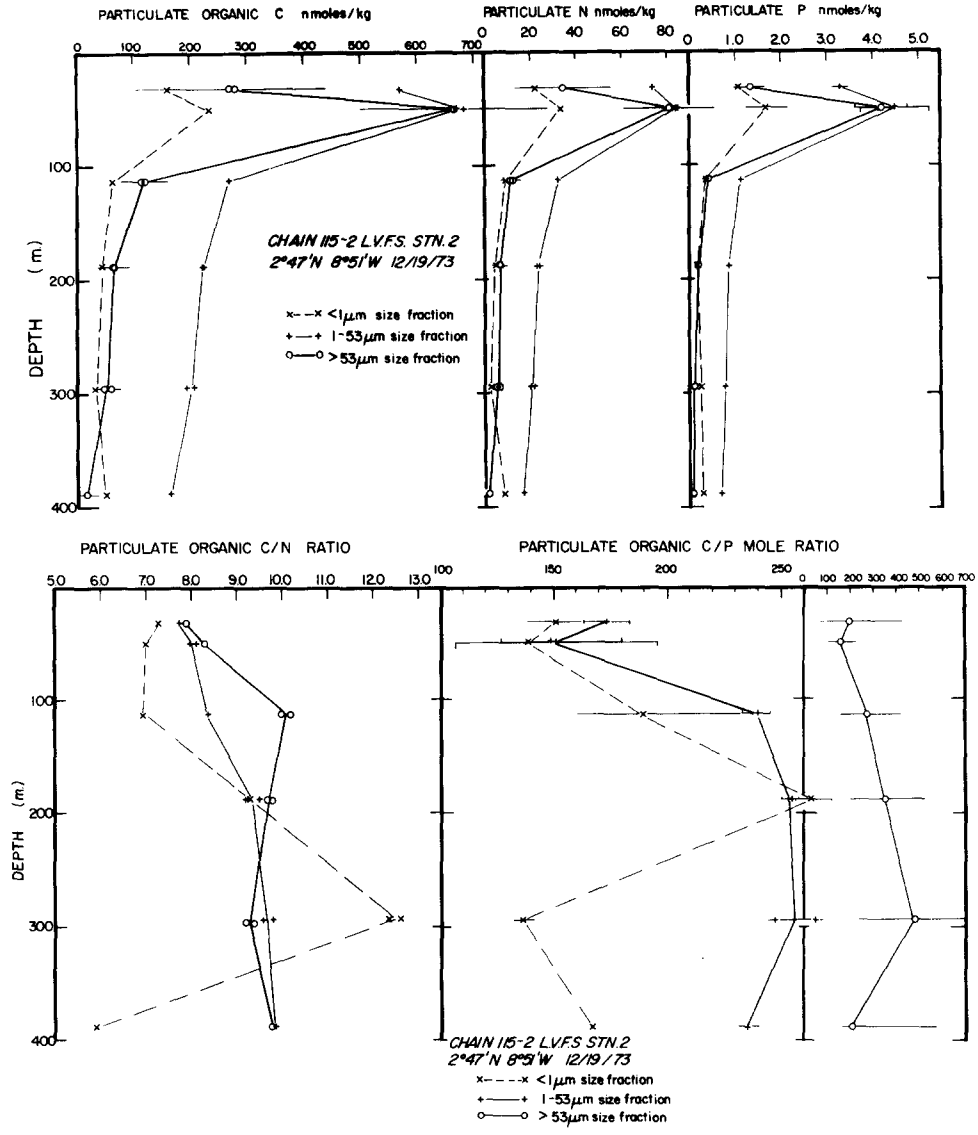

Fig. 5. Upper: C_{org}, N, and P profiles for the <1-, 1- to 53-, and >53-μm size fractions. The concentration gradients between 50 and 113 m are largest for >53-μm and smallest for <53-μm particles, indicating that grazing organisms strongly influence the particle distributions over this depth interval. Two points indicate replicate analyses. Lower: organic C/N and C/P ratios showing size and depth-dependent behavior. Large error bars of the >53-μm C/P ratio are due to uncertainty in the recovery of material removed from the filter for C and N analysis.

Bacteria may account for a significant fraction of the material in the <1-μm fraction. As elemental composition data are rare for marine bacteria (VINOGRADOV, 1953) the data for terrestrial species will be taken as typical: C/N = 5; C/P = 50 to 100 (PORTER, 1946; LURIA, 1961). Bacteria are predominantly in association with phytoplankton (SVERDRUP, JOHNSON and FLEMING, 1942; SOROKIN, 1973) and are frequently associated with maxima in zooplankton (YOUNGBLUTH, 1975), chlorophyll, and particulate matter at the base of

the mixed layer (SOROKIN, 1973). Their presence could explain the lower C/N and C/P ratios in the < 1-μm fraction than in the larger fractions.

In the 1- to 53-μm fraction the C/N ratio increases steadily below 32 m, indicating a 20% preferential loss of N relative to organic C. In contrast, phosphorus is 40% depleted relative to carbon between 50 and 113 m and shows little further relative loss below this depth. In the > 53-μm fraction 20% of the N and 50% of the P is lost relative to organic carbon between 50 and 113 m with little further change. It can be concluded that phosphorus is more easily lost from the organic fraction than nitrogen.

The $\delta^{13}C$ analyses were made because it was thought that the values would be a useful indicator of the organic composition of the particulate material. Labile components such as amino acids have been shown to be ^{13}C-rich relative to refractory organic

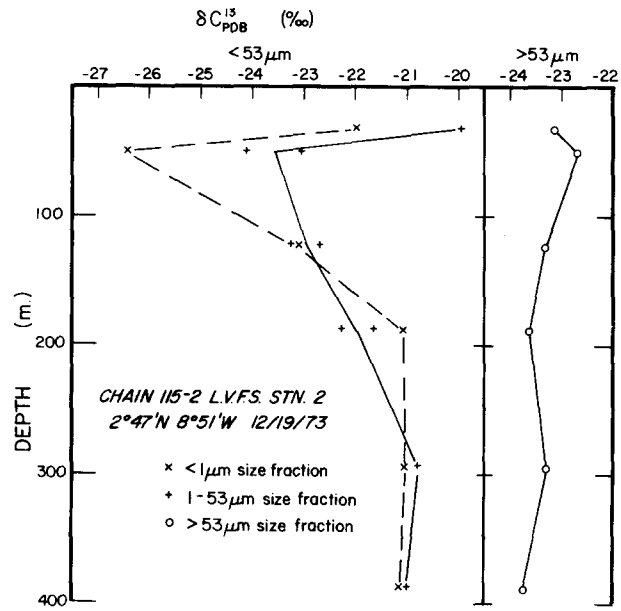

Fig. 6. $\delta^{13}C_{PDB}$ profiles for organic carbon in the three size fractions. The strong (−4‰) fractionation between 32 and 50 m in the <1- and 1- to 53-μm size fractions is probably due to the presence of bacteria.

components such as cellulose or 'lignin' (DEGENS, BEHRENDT, GOTTHARDT and REPPMAN, 1968; WILLIAMS and GORDON, 1970).

The particulate data (Fig. 6) are complex. The < 53-μm fractions both show a depletion in ^{13}C of 4‰ over the depth interval between 32 and 50 m. The > 53-μm fraction shows an increase of 0.7‰ in the same interval. This behavior is unrelated to the C/N and C/P ratios, which are invariant. The $\delta^{13}C$ data for the < 53-μm fractions are not an artifact of filter washing because the < 53-μm samples analyzed at LVFS Sta. 1 (unwashed) exhibit similar behavior. Nor do temperature effects (SACKETT, ECKELMAN, BENDER and BÉ, 1965), kinetic effects (DEUSER, DEGENS and GUILLARD, 1968), and species differences in plankton (SACKETT, EADIE and EXNER, 1973) explain the variations observed at this station.

A marine bacterium *Nitrosocystis* cultured at 20°C was determined to have $\delta^{13}C = -35.7‰$ (DEGENS, GUILLARD, SACKETT and HELLEBUST, 1968). If all marine bacteria exhibit the same ^{12}C enrichment and are an important component of the < 53-μm fractions at 50 m, then it can be calculated that they comprise approximately 45 and 20%

of the organic carbon present in the < 1- and 1- to 53-μm fractions at 50 m. SOROKIN (1973) reported bacterial biomasses in the tropical Pacific (7°N, 135°E; upper 250 m) in the range between 200 and 950 nmoles $C_{org}\,kg^{-1}$ of seawater, consistent with the LVFS data. The presence of marine bacteria in the < 1-μm and 1- to 53-μm size fractions accounts for the observed $\delta^{13}C$ and for the CNP values. The interpretation of the character of the organic compounds present is therefore ambiguous. The carbon isotope variations in the particles at this station are quite unlike those reported by EADIE and JEFFREY (1973); the reasons for this difference are unknown.

Major ions: calcium, magnesium, and potassium

The uptake and transport by particles of the major ions of seawater are extremely difficult to study using the dissolved distributions of these elements in the water column. There have been no well-documented cases reported for the non-conservative behavior of Na, K, and Mg in the water column (MANGELSDORF and WILSON, 1972). Ca and Sr show a maximum of 1% variation relative to salinity (HORIBE, ENDO and TSUBOTA, 1974; BRASS and TUREKIAN, 1974). The study of these elements in particles is essential to understanding the mechanisms affecting their distributions in the water column.

Table 7 and Fig. 7 summarize the particulate distributions of calcium and carbonate in the water column. The > 53-μm fraction contains 30 and 10% of the total above and below 100 m, respectively. Light microscopic and SEM studies show that whole organisms account for most of the carbonate at 32 and 50 m, whereas fragments dominate below 50 m in both the 1- to 53-μm and > 53-μm size fractions. Furthermore, calcium carbonate is the dominant calcium phase in the particles accounting for greater than 80% of the acid leachable calcium; any calcium in excess of carbonate is termed 'excess'. The Ca^{2+}/CO_3^{2-} and excess calcium profiles (Fig. 7) show that excess calcium is rapidly lost from the > 53-μm fraction in the upper 100 m. The 1- to 53-μm fraction shows excess calcium, particularly at 294 m. The excess calcium in the samples above 100 m is probably contained in the cytoplasm of living organisms as the C_{org}/Ca ratios are typical for plankton ($C_{org}/Ca = 160$; MAYZAUD and MARTIN, 1975); the excess calcium at 294 m in the 1- to 53-μm fraction is high ($C_{org}/Ca = 30$).

The LVFS samples consistently contain particulate magnesium. Correction of the total magnesium content of the filters for blank and sea salt (using the Na data) always leaves a residual amount of magnesium (defined as 'excess' magnesium). In many cases this excess magnesium is several times the blank levels (Table 3). Particulate magnesium has been reported in the deep water of the Gulf of Mexico (FEELY, 1975), and in the North Atlantic by SPENCER, BREWER and BENDER (in press). The values of 'excess' magnesium leachable by acid (FEELY, 1975) and total magnesium (SPENCER, BREWER and BENDER, in press) are similar, suggesting that the bulk of particulate magnesium is acid leachable.

Like excess calcium, excess magnesium in the > 53-μm size fraction shows a maximum at 50 m; unlike excess calcium, excess magnesium is present in the particles below 100 m. In the 1- to 53-μm size fraction the profiles of excess magnesium and calcium are similar and, relative to organic carbon, excess magnesium is progressively enriched with depth from a mole ratio of 0.4% to approximately 2% in both size fractions.

FEELY (1975) suggested that excess magnesium is present in particles as $MgCO_3$. However, the Mg^{2+}/CO_3^{2-} mole ratio is 20 and 10% above and below 100 m, respectively, in both size fractions, much greater than the reported values for coccoliths (0.4%, THOMPSON and BOWEN, 1969) and Foraminifera (0.5%, EMILIANI, 1955), which are the

Table 7. Particulate calcium, carbonate, magnesium, potassium, silicon and strontium data (nmoles kg^{-1}). Upper: > 53-μm size fraction. Lower: < 53-μm size fraction.

z		C_i	Ca	xs Ca	$\overline{C_i}/\sigma_{C_i}$	$\overline{Ca}/\sigma_{Ca}$	$Ca_{xs}/\sigma_{Ca_{xs}}$		Na	xs Mg	$\overline{Mg}_{xs}/\sigma_{Mg_{xs}}$	K_{xs}	$\overline{K}_{xs}/\sigma_{K_{xs}}$	Sr	$\overline{Sr}/\sigma_{Sr}$	$\overline{Sr}^*$		Si	$\overline{Si}/\sigma_{Si}$
32	a	6.36	7.43	1.07	6.8 /0.6	8.5 /1.2	1.7 /1.4	a	33.4	1.14	1.17/0.13	0.77	0.63/0.12		0.674/0.000	0.663	d	6.14	6.5/0.6
	a	7.26	-					a	-			-					e	6.93	
	b		8.28					b	40.6	1.06		-		0.674					
	c		9.78					c	26.2	1.30		0.53		0.674					
50	a	9.29	11.49	2.20	10.1 /1.1	12.3 /0.7	2.3 /1.3	a	8.55	2.17	2.23/0.11	0.50	0.73/0.20		1.13 /0.11	1.11	d	25.27	25.6/0.4
	a	10.80	12.31	1.51				a	19.1	2.37		0.84					e	25.90	
	b		12.20					b	17.8	2.25		-		1.045					
	c		13.18					c	14.5	2.12		0.84		1.205					
113	a	7.49	7.62	0.13	7.5 / -	7.7 /0.6	0.2 /0.6	a	3.48	0.41	0.47/0.14	0.04	0.03/0.01		0.123/0.023	0.110	d	10.75	10.5/0.3
	b		7.18					b	1.19	0.38		-		0.106			e	10.27	
	c		8.30					c	2.01	0.63		0.02		0.139					
188	a	4.03	4.08	0.05	4.2 /0.2	4.4 /0.4	0.25/0.4	a	2.78	0.32	0.37/0.06	0.01	0.014/0.02		0.078/0.029	0.072	d	5.76	7.0/1.8
	a	4.28	4.17	-0.11				a	3.02	0.31		0.03					e	8.29	
	b		4.91					b	3.52	0.43		-		0.099					
	c		4.73					c	5.78	0.42		0.00		0.058					
294	a	4.12	4.17	0.05	4.7 /0.8	4.7 /0.4	0.1 /0.9	a	2.06	0.38	0.37/0.08	0.01	0.04/0.04		0.042/0.015	0.034	d	5.10	5.2/0.1
	a	5.20	5.10	-0.10				a	4.31	0.45		0.09					e	5.23	
	b		4.91					b	2.00	0.27		-		0.053					
	c		4.73					c	1.64	0.38		0.02		0.032					
388	a	3.11	3.18	0.07	3.0 /0.2	3.4 /0.6	0.4 /0.6	a	1.02	0.27	0.26/0.01	-0.02	0.00/0.03		0.043/0.003	0.038	d	3.64	4.1/0.7
	a	2.85	2.83	-0.02				a	0.88	0.27		-0.02					e	4.58	
	b		3.30					b	2.97	0.25		-		0.045					
	c		4.14					c	1.82	0.26		0.03		0.041					
32	a	13.1	b	13.9	13.9 /1.1	13.3 /0.9	-0.6/1.4	b	106.6	0.3	2.5 /3.1			0.35	0.30 /0.07	0.28	f	20.8	
	a	14.6	c	12.7				c	120.0	4.7				0.25					
50	a	15.8	b	18.5	15.8 / -	17.7 /1.1	1.9/1.1	b	136.0	1.5	2.7 /1.7			0.32	0.30 /0.02	0.28	f	28.4	
			c	17.0				c	134.0	3.9				0.29					
113	a	51.1	b	58.5	50.3 /0.7	55.6 /4.2	5.3/4.3	b	21.6	2.2	2.15/0.07			0.39	0.40 /0.01	0.31	f	32.2	
	a	50.0	c	52.6				c	21.5	2.1				0.41					
	a	49.7																	
	a	49.8	a	51.0															
188	a	35.4	b	39.6	35.6 /0.3	37.2 /2.6	1.6/2.6	b	39.0	1.7	1.9 /0.6			0.226	0.218/0.007	0.156	f	18.0	
	a	35.8	b	34.4				b	34.2	1.4				0.214					
			c	37.5				c	34.9	2.5				0.215					
294	a	35.4	b	42.6	35.0 /0.6	40.4 /3.0	5.4/3.1	b	21.8	4.4	3.6 /1.1			0.185	0.190/0.007	0.131	f	22.8	
	a	35.8	c	38.2				c	14.4	2.8				0.195					
388	a	30.4	b	32.3	30.4 /0.0	33.0 /1.0	2.6/1.0	b	135.6	1.2	0.4 /1.6			0.116	0.109/0.006	0.053	f	13.8	
	a	30.4	b	32.7				b	156.9	1.5				0.106					
			c	34.2				c	70.8	-1.4				0.106					

a, 20% H_3PO_4. b, 2.2 M acetic acid. c, 0.6 N HCl. d, 1 N NaOH. e, 0.4 M Na_2CO_3. f. 10 N NaOH, 0.4 μm Nuclepore filter.

C_i—carbonate carbon. $Sr^* = Sr - 0.0017C_i$ = non-carbonate Sr.

Means/standard deviations are calculated for multiple analyses.

xs—remaining element after filter blank and seasalt corrections (Mg, K, Sr) and carbonate correction (Ca).

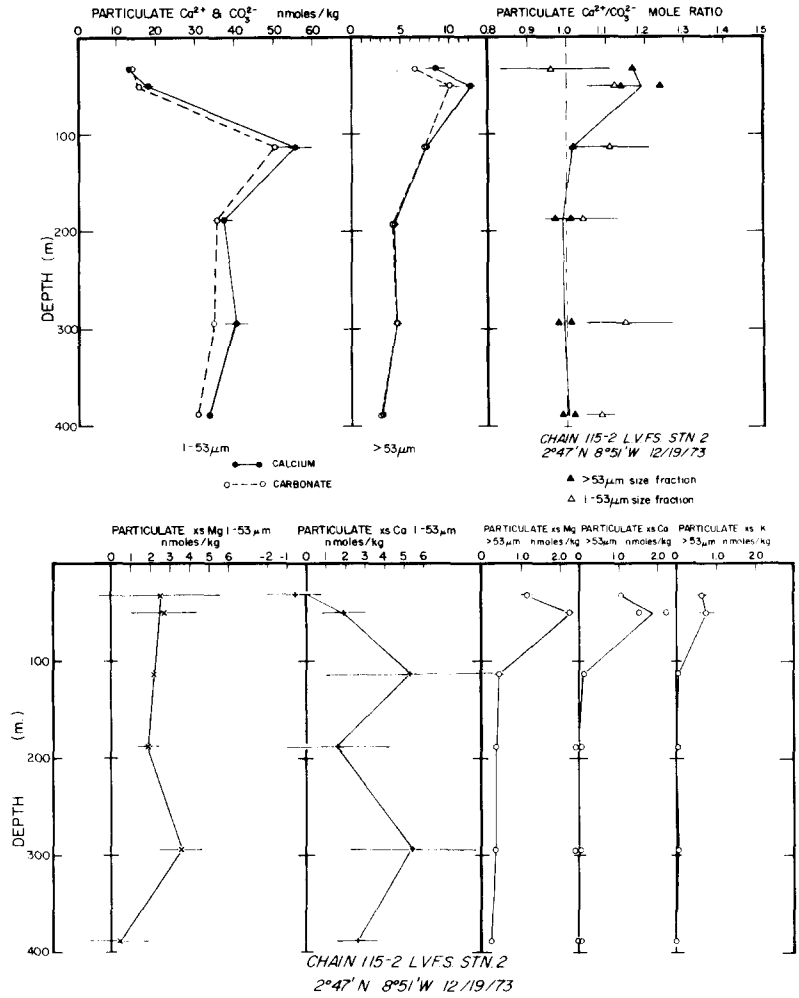

Fig. 7. Upper: calcium and carbonate in the 1- to 53-μm and > 53-μm size fractions showing excess calcium. Lower: excess magnesium, calcium, and potassium in the two size fractions. Excess Mg and K are the remaining anomalies in the Mg and K data after correction for filter blank and sea salt (using Na data); excess Ca is the anomaly after filter blank, sea salt, and $CaCO_3$ are subtracted.

major carbonate phases in both size fractions. Hence carbonate cannot be the major magnesium phase.

Excess potassium is lost from the > 53 μm particles in the upper 100 m and behaves like excess calcium, being typically found in the cytoplasm of organisms (HUGHES, 1972). Potassium was not determined in the < 53-μm fraction because the blank levels were highly variable and exceeded the amounts of potassium expected in the particles.

Ion exchange and acid leaching experiments

A series of experiments was designed to test whether or not the excess calcium and magnesium in the 1- to 53-μm fraction at 294 m were bound by ion exchange.

Two 45-mm diameter disks were cut from the top glass fiber filter of this sample (chosen because it had the greatest excess Ca and Mg) and tightly clamped in an acid-leached distilled water-rinsed 47-mm Millipore® glass filtration apparatus (effective filtration diameter 35 mm). One hundred milliliters of $10^{-4.5}$ N NaOH solution were allowed to drip through the filter pair to dissolve the residual sea salt. Additional 10-ml aliquots of this solution were allowed to drip through the sample, each for approximately 1 min before the remaining solution was sucked through the filter using reduced pressure; each aliquot was saved for later analysis. Then fourteen 10-ml aliquots of 0.05 M $MgCl_2$ (in $10^{-4.5}$ N NaOH) were allowed to drip through the filters in the same fashion. An identical sequence of washes was used to treat two 45-mm disks cut from the bottom glass fiber filter of the 294-m sample. Ten milliliters of the $MgCl_2$ solution were added to the $10^{-4.5}$ N NaOH aliquots and similarly 10 ml of $10^{-4.5}$ N NaOH were added to the $MgCl_2$ aliquots. Calcium, strontium, and potassium standards were prepared in the same $MgCl_2$–NaOH matrix solution and all aliquots and standards were analyzed for these elements by flame atomic absorption spectroscopy.

The cumulative analyses for Ca, Sr, and K are plotted against cumulative rinse solution volume (Fig. 8). The first aliquot of the 0.05 M $MgCl_2$ rinse solution was greatly enriched in calcium and strontium relative to aliquots immediately preceding and following it (Fig. 8). The plots of cumulative Ca and Sr exhibit a sharp increase coinciding with the first $MgCl_2$ aliquot. The cumulative plots then become linear upon completion of ion-exchange. The quantity of ion-exchanged cations is calculated by extrapolating the linear portions of the cumulative plots to the point of the first $MgCl_2$ aliquot. The vertical separation of the two lines at this point divided by the area fraction of the filter subsample gives the total quantity of cations bound by ion-exchange for the whole filter. The con-

Table 8. Ion exchange experiments pH > 8 (*Chain* 115-2 LVFS Sta. 2, < 53-μm sample, z = 294 m).

EXPT	SAMPLE	WASH SOL^N	pH(NaOH)	millimoles of cations exchanged				EXC. meq.
				Mg^{2+}	Ca^{2+}	Sr^{2+}	K^+	
1	"TOP"	0.05 M $MgCl_2$	9.5	WASH	0.142	0.00066	<0.005	0.291
2	"BOTTOM"	0.05 M $MgCl_2$	9.5	SH	0.0097	0.00002	<0.001	0.0204
1-2	NET EXCHANGE			-	0.132	0.00064	< .004	0.271
3	NEW "TOP"	0.05 M $CaCl_2$	8.3	0.018	WASH	Blank levels		0.036
4	NEW "BOTTOM"	0.05 M $CaCl_2$	8.3	0.020	SH	too high		0.040
3-4	NET EXCHANGE			-0.002	-	-	-	-0.004
5	FROM 3	0.1 M NaCl	8.3	0.0026	>.128	0.0002	-	>0.261
6	FROM 4	0.1 M NaCl	8.3	0.0013	0.0296	0.0000	-	0.062
5-6	NET EXCHANGE			+0.0013	>0.0984	0.0002	-	>0.199
1,3	SUMMARY TOP			0.0206	0.142	0.00066	< .005	0.331
2,4	SUMMARY BOTTOM			0.0213	0.0097	0.00002	< .001	0.063
	SUMMARY NET EXCHANGE			-0.0007	0.132	0.00064	< .004	0.268
	ION-EXCHANGED n moles/kg			-0.03	6.1	0.032	0.18	
	OBSERVED n moles/kg			3.6 ± 1.1	5.4 ± 3.1	0.19	-	
	ION-EXCHANGED/OBSERVED			-0.02	1.13	0.17	-	

Mg is *not* exchanged under these conditions at least 70% of excess Ca is ion-exchanged and 17% of total Sr is ion-exchanged.

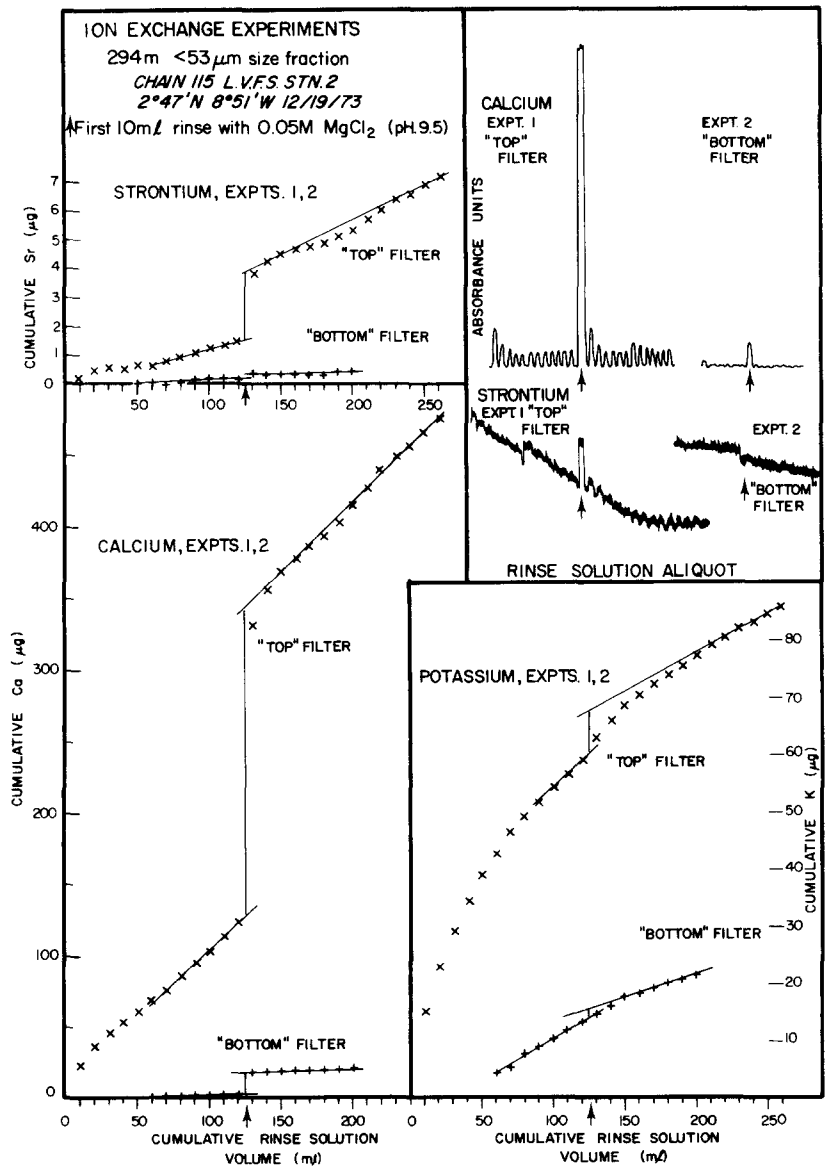

Fig. 8. Ion exchange experiments for calcium, strontium, and potassium. The chart recorder output from the flame atomic absorption analyses of the rinse solutions for calcium and strontium is shown in the upper right portion of the figure. The $10^{-4.5}$ N NaOH aliquots are to the left of the big peak which corresponds to the first 0.05 M $MgCl_2$ in $10^{-4.5}$ N NaOH aliquot. 'Top' and 'Bottom' correspond to 1- to 53-μm and <1-μm samples from 294 m. The rest of the figure shows the cumulative data plots used to calculate the ion-exchangeable Ca, Sr, and K in the sample. 1/26th of the filter was used for these experiments.

centration of cations ion-exchanged on the particles is the difference between the values for the top and bottom glass fiber filter samples. The results of these experiments are summarized in Table 8.

A similar experiment for Mg was carried out on separate filter samples using $10^{-5.7}$ N NaOH aliquots and 0.05 M $CaCl_2$ in $10^{-5.7}$ N NaOH aliquots (Table 8, Exps. 3 and 4).

Total exchange capacity of the material was determined in another experiment in which the calcium was ion-exchanged with 0.1 M NaCl in $10^{-5.7}$ N NaOH solution (Exps. 5 and 6).

The results of Exps. 1 to 4 showed that $107 \pm 37\%$ of the excess calcium and 17% of the total strontium was bound by ion exchange; little potassium and *no* magnesium were so bound. The total ion-exchange capacity of the particles inferred from these results was 96 mequiv $(100\,g)^{-1}$. Experiments 5 and 6 have identical results for the exchange capacity of the bottom filter, but gave an exchange capacity for the particles on the top filter of 71 mequiv $(100\,g)^{-1}$. This result could be low for two reasons: possible degradation of the organic matter that may be the ion-exchanger and increased rate of dissolution of $CaCO_3$ because of the lower pH (8.3) used in Exps. 3 to 6.

Aluminosilicate material cannot make an important contribution to the ion exchange capacity of the particles of this sample since over 90% of the total dry weight of the material is biogenic (Table 4). The surface sediments below Sta. 2 are typically 40% kaolinite, 30% illite, 20% montmorillonite, and 10% chlorite in the < 2-μm carbonate free fraction (GOLDBERG and GRIFFIN, 1964). The ion exchange capacity of this material is calculated to be 22 mequiv $(100\,g)^{-1}$ (BEAR, 1964). The maximum contribution by aluminosilicates to the total exchange capacity of the particles is therefore less than 3 mequiv $(100\,g)^{-1}$.

BEAR (1964) has shown that the ratio of monovalent to divalent cations bound on an ion-exchanger in equilibrium with a solution of constant relative ionic composition is a function of the ionic strength of that solution. Ion-exchangers take up divalent in preference to monovalent cations as the ionic strength of the solution is decreased. Washing the particulate matter with distilled water may have changed the relative amounts of bound cations; however, the analyses of the samples from Chain 115-2 LVFS Sta. 1 revealed excess calcium ranging from 2 to 6 nmole kg^{-1} below 50 m, indicating that the effect is real and not an artifact of the filter washing.

The samples used in Exps. 3 to 6 were treated with additional rinse aliquots: $10^{-5.7}$ N NaOH (pH = 8.3), laboratory distilled water (pH 5.5), and 10^{-3} N HCl (pH = 3.0) to determine the conditions necessary for the release of the particulate magnesium. The Mg/Ca ratios measured in the wash aliquots from Exp. 5 varied between 1.5 and 2 mole %. The pH 8.3 aliquots from this series of experiments showed an initial value of 14% with subsequent aliquots falling between 3 and 6%; rinse aliquots at pH 5.5 showed little change in the Mg to Ca mole ratio; aliquots of the pH 3 solution showed sharp increase in the magnesium concentration relative to previous aliquots and the Mg/Ca mole ratio rose from 6 to over 30% and fell back to values of near 16%. From the point of the first pH 3 aliquot, a total of 28 μg of magnesium was lost from the filter subsample, equivalent to 0.8 mg of magnesium lost from a full sized filter corresponding to approximately 40% of the excess magnesium observed at 294 m in the 1- to 53-μm fraction. This experiment, although not quantitative, clearly demonstrates that Mg is not present in particulate matter as carbonate. The loss of Mg from the particles proceeds extremely slowly at pH 5.5 and it is only at pH 3 that most of the magnesium (in excess of the filter blank) is lost from the particles. Phosphate analysis of the pH 3 rinse solutions showed no phosphate accompanying the magnesium. In living organisms magnesium is used in DNA synthesis and some enzymatic reactions; magnesium is bound in the porphyrin ring of chlorophylls and is possibly important in maintaining the structure of cell walls (HUGHES, 1972). The particulate C_{org}/Mg mole ratio in the surface waters is 250/1 and compares well with the plankton analyses of MAYZAUD and MARTIN (1975), $C_{org}/Mg = 350$. The C_{org}/Mg ratio

decreases to values between 100 and 50 below 200 m. If Mg is organically bound, then its carrier is progressively enriched in the organic material in both size fractions. It is unlikely that aluminosilicates are a source for the magnesium because their structures should not be degraded by the chemical conditions of this experiment.

BREWER, WONG, BACON and SPENCER (1975) have postulated that the oxidation of 1 mole of REDFIELD–KETCHUM–RICHARDS (1963) model plankton $[(CH_2O)_{106}(NH_3)_{16}(H_3PO_4)_1]$ would yield 16 moles of nitric acid which would 'titrate' the seawater in the deep ocean and lower its alkalinity. Table 9 lists the depth dependence of the cation composition of the organic matter in both size fractions normalized to 106 atoms of carbon (the number used in Redfield model plankton). The table shows that both size fractions at 32 and 50 m are low in cation content; the ratio of total equivalents of cations to nitrogen is in the range of 0.07 to 0.13 for these samples. Below 50 m, this

Table 9. C_{org}, N, P, cation relationships in particles normalized to 106 atoms of C. Upper: > 53-μm size fraction. Lower: 1- to 53-μm size fraction.

Z	C_o	N	P	$xs\overline{Ca}/\sigma_{xsCa}$	$xs\overline{Mg}/\sigma_{xsMg}$	$xs\overline{K}$
32	106	13.3	0.51	0.41/ -	0.45/.05	0.24
50	106	12.9	0.67	0.30/.08	0.36/.02	0.12
113	106	10.5	0.37	0.12/ -	0.43/.13	0.03
188	106	10.9	0.29	-0.05/.19	0.61/.11	0.02
294	106	11.1	0.21	-0.05/.19	0.70/.15	0.08
388	106	10.7	0.40	0.17/.43	1.75/.06	0.00
32	106	13.7	0.61	-0.11/0.15	0.50/0.54	-
50	106	13.2	0.71	0.30/0.17	0.42/0.27	-
113	106	12.7	0.44	2.10/1.70	0.85/0.03	-
188	106	11.3	0.42	0.77/1.24	0.91/0.27	-
294	106	11.0	0.41	2.85/1.64	1.90/0.58	-
388	106	10.7	0.45	1.68/0.64	0.28/1.03	-

ratio has the range 0.11 to 0.36 (0.18, average), for the > 53-μm fraction, and 0.30 to 0.86 (0.50 average) for the 1- to 53-μm fraction. These data show that cations are an important component of the organic fraction in the deeper samples.

If we assume that the > 53-μm particles are reactive within the water column, then our data indicate that the reduction of alkalinity due to oxidation of organic matter is 80% of that proposed by BREWER *et al.* (1975). Similarly, for the 1- to 53-μm particles, the reduction of alkalinity would be only 50% of that proposed. This compensating effect is because cations occupy negative sites on organic matter instead of protons. We have demonstrated that there is a change in the C, N, P, and cation content of the particulate matter within the upper 400 m of the water column. It is there that the major anomalies of calcium and alkalinity probably occur.

Silicon

Figure 9 shows the particulate Si profiles for the > 53-μm fraction and for the 0.4-μm Nuclepore filtered samples. The 'bulk' suspended silicate concentration determined by Nuclepore filtration of 20-l samples is approximately 20 to 30 nmole kg^{-1} and compares

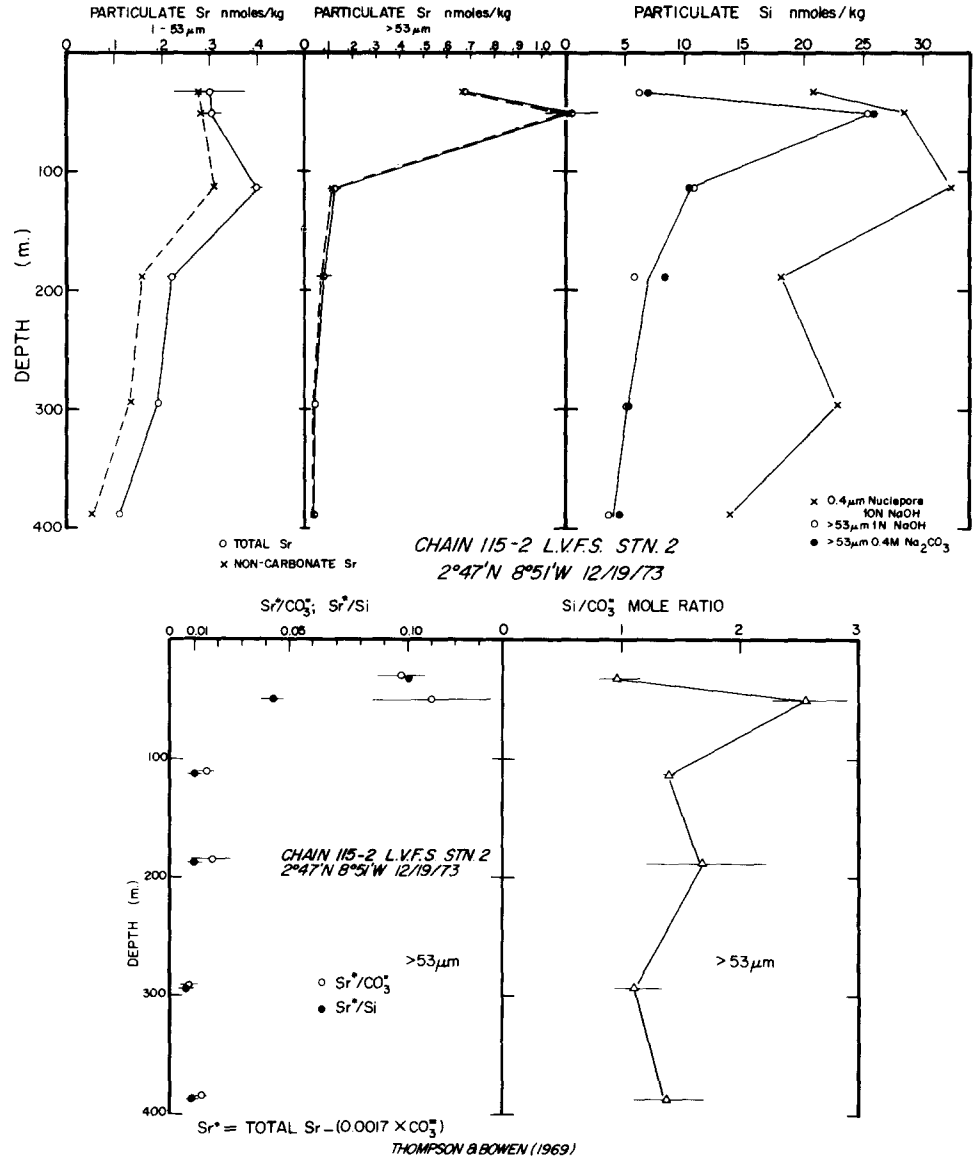

Fig. 9. Upper: silicate in >53-μm fraction and from 0.4-μm Nuclepore filter samples; total strontium and non-carbonate strontium (Sr*) in >53- and <53-μm fractions. Lower: strontium (Sr*), carbonate, and silicate ratios in >53-μm size fraction.

well with the lowest particulate silicate values (range 19 to 580 nmoles Si kg^{-1}, mean 110 nmoles Si kg^{-1}) reported by COPIN-MONTEGUT and COPIN-MONTEGUT (1972). The difference between the analyses of the 0.4-μm Nuclepore filters and the >53-μm fraction is considered to be representative of the 1- to 53-μm fraction, especially in the near-surface samples. Therefore it is inferred that the 1- to 53-μm Si profile has the same characteristics as the 1- to 53-μm carbonate profile with the exception of the 32-m sample. SEM showed whole diatoms to be the most abundant contributors to opaline silica in the 1- to 53-μm

fraction at 32 and 50 m, whereas diatom fragments predominate in the deeper samples. The results of the 1.0 N NaOH and 0.4 M Na_2CO_3 analyses of the > 53-μm fraction were identical.

Strontium

Particulate strontium occurs in three phases: carbonate, celestite, and organics. THOMPSON and BOWEN (1969) and EMILIANI (1955) showed coccolith ooze and Foraminifera to contain 0.17 mole% Sr. Total strontium analyses were corrected using the carbonate data and the above factor to give non-carbonate strontium, Sr*.

$$Sr^* = \text{Total Sr} - 0.0017\,(\text{carbonate}). \quad (1)$$

From Fig. 9 the 1- to 53-μm fraction is progressively depleted in Sr* with increasing depth to less than 50% of the total. However, the > 53-μm fraction is composed mainly of non-carbonate strontium. Celestite ($SrSO_4$) is the major structural component of Acantharia (BOTTAZZI *et al.*, 1971). SEM and light microscopic studies showed the > 53- and < 53-μm fractions to contain whole Acantharia and their fragments, respectively.

It was suggested above that 17% of the total strontium in the 1- to 53-μm fraction is bound in ion-exchangeable positions on the organic matter at 294 m. This may occur at other depths as well.

Celestite is extremely soluble in seawater; BRASS and TUREKIAN (1974) suggest from profile data that Sr is involved in a shallow regenerative cycle similar to phosphate. Thus the order-of-magnitude decrease of the Sr*/Si and Sr*/$CaCO_3$ ratios with depth (Fig. 9) may arise largely from the dissolution of $SrSO_4$. However, the Sr*/Si and Sr*/$CaCO_3$ profiles also reflect the transfer of carbonate, opal, and celestite between the < 53- and > 53-μm fractions. Unlike Acantharia (celestite), which occur only in the > 53-μm fraction, coccolithophorids (carbonate) and diatoms (opal) are found in the < 53-μm fraction. The action of filter feeding organisms transfers diatom and radiolarian (opal), foraminiferan (carbonate), and acantharian (celestite) components to the 1- to 53-μm fraction by fragmentation; at the same time, the > 53-μm fraction becomes enriched with coccoliths and diatom fragments by aggregation (see below). Thus, loss of strontium from the > 53-μm size fraction by dissolution (and fragmentation) and gain of small carbonate and opal particles from the < 53-μm fraction together determine the Sr*/Si and Sr*/$CaCO_3$ ratios in the > 53-μm fraction as a function of depth. In contrast, the Si/$CaCO_3$ mole ratio in the > 53-μm fraction is essentially constant (approximately 1.0) except at 50 m, where an increased population of diatoms and Radiolaria exists.

If dissolution of $SrSO_4$ were the primary process governing the Sr*/$CaCO_3$ and Sr*/Si ratios, then a dramatic change in the preservation of the Acantharia should occur between 50 and 113 m. The SEM showed the Acantharia at 32 and 50 m to be well preserved except for mechanical damage (Fig. 10 A to F). At 113 m (Fig. 10 G to I) most acantharian structures were virtually undamaged except by breakage, but the organic membrane seen to be coating the spines of the Acantharia at 32 and 50 m was absent in many cases. There is some etching of the spines of a few Acantharia sampled at this depth (Fig. 10 H to I), but the extent of dissolution is almost negligible; i.e. ~1%. At 188 m (Fig. 11 A to C) there is a larger proportion of mechanically damaged Acantharia and some spines clearly show the effects of dissolution (Fig. 11 B to C); a double point structure is observed at the ends of the etched spines. Well-preserved Acantharia are common and the extent of dissolution at 188 m is estimated to be only 10%. At 294 m some Acantharia (Fig. 11

D to G) are poorly preserved with the 'double point' etching pattern having progressed almost the whole length of some spines; an estimated 20 to 40% dissolution has occurred at this depth. Finally, at 388 m some Acantharia are barely recognizable because of the almost complete dissolution of their spines (Fig. 11I). A few relatively well-preserved Acantharia are also observed at this depth (e.g. Fig. 11H); close examination of their spines also shows the beginnings of the double point etching pattern. Between 50 and 75% of the strontium has been dissolved from the Acantharia above 400 m, with most dissolution occurring below 200 m. Thus the strong gradient in the $Sr^*/CaCO_3$ and Sr^*/Si mole ratios between 50 and 113 m is not due to the dissolution of $SrSO_4$ but to the transfer of carbonate, opal, and celestite fragments between the < 53- and > 53-μm fractions.

Iron

The concentrations of iron in the 1- to 53- and >53-μm fractions are highest at 32 m; only the < 1-μm fraction exhibits the 50-m maximum. The Fe values (hydroxylamine-hydrochloride, hydrochloric acid leach, Table 10, Fig. 12) average $4.4 \pm 1.5(\sigma)$ nmoles

Table 10. Particulate iron (nmoles kg^{-1}) and particulate radioisotope activities [dpm $(100\,kg)^{-1}$].

z (m)	Fe <1μm	Fe 1-53μm	Fe >53μm	$^{210}Pb/\sigma$ <1μm	$^{210}Pb/\sigma$ 1-53μm	$^{210}Pb/\sigma$ >53μm
32	1.69	3.79	1.32	0.38/.03	0.60/.04	0.181/.013
50	2.09	2.02	1.06	0.24/.03	0.33/.04	0.153/.012
113	0.86, 0.88	1.86, 1.77	0.436	0.012/.006	0.54/.03	0.083/.005
188	0.35	1.96	0.330	0.014/.004	0.46/.03	0.072/.005
294	0.46, 0.46	3.29, 3.58	0.401	0.006/.004	0.54/.03	0.063/.004
388	0.47	3.33	0.360	0.001/.004	0.43/.03	0.041/.004

z (m)	$^{7}Be/\sigma$ 1-53μm	$^{214}Pb/\sigma$ 1-53μm	$^{214}Bi/\sigma$ 1-53μm	$^{210}Po/\sigma$ <1μm	$^{210}Po/\sigma$ 1-53μm
32	2.3/1.0	<0.03	<0.08	0.4/.10	1.00/.10
50	4.1/1.5	<0.05	<0.10	0.15/.09	0.80/.10
113	<0.05	0.18/.02	0.19/.022	0.06/.03	0.31/.07
188	<0.2	0.22/.03	0.17/.046	0.03/.02	0.43/.08
292	<0.2	0.075/.021	0.086/.032	0.12/.02	0.69/.09
388	<0.2	0.082/.020	0.072/.020	0.06/.02	0.62/.07

* Autoclave 18 h 0.6 N HCl, 0.15 M $NH_2OH \cdot HCl$ replicates are indicated.

Fe kg^{-1} and compare well with the values [Instrumental Neutron Activation Analysis (INAA) of samples from 30-l. Niskin samplers] of SPENCER and BREWER (unpublished data report) of $4 \pm 2.6(\sigma)$ nmoles Fe kg^{-1} for the upper 400 m at Geochemical Ocean Sections Program (GEOSECS) Sta. 40 (4°N, 38°W). In preliminary work determining the best conditions for particulate iron analysis, it was found that the shapes of the particulate iron particles were the same using much milder conditions (0.6 N HCl, 24 h, 25°C) even though the values for particulate iron were an order of magnitude lower. The < 1-μm fraction exhibits a nearly uniform Fe/P mole ratio of 1.8 ± 0.5; in the larger size fractions, the Fe/P ratio varies by an order of magnitude, being lowest (0.25) at 50 m and highest (4 to 5) below 200 m and indicating the refractory nature of the particulate iron.

Radioisotopes ^{210}Pb *and* ^{210}Po, ^{7}Be

The analyses of particulate ^{210}Pb ($t_{1/2} = 22$ yr), ^{210}Po ($t_{1/2} = 138$ day) and ^{7}Be ($t_{1/2} = 53$ day) were undertaken with the idea that their activities may be used to assign average

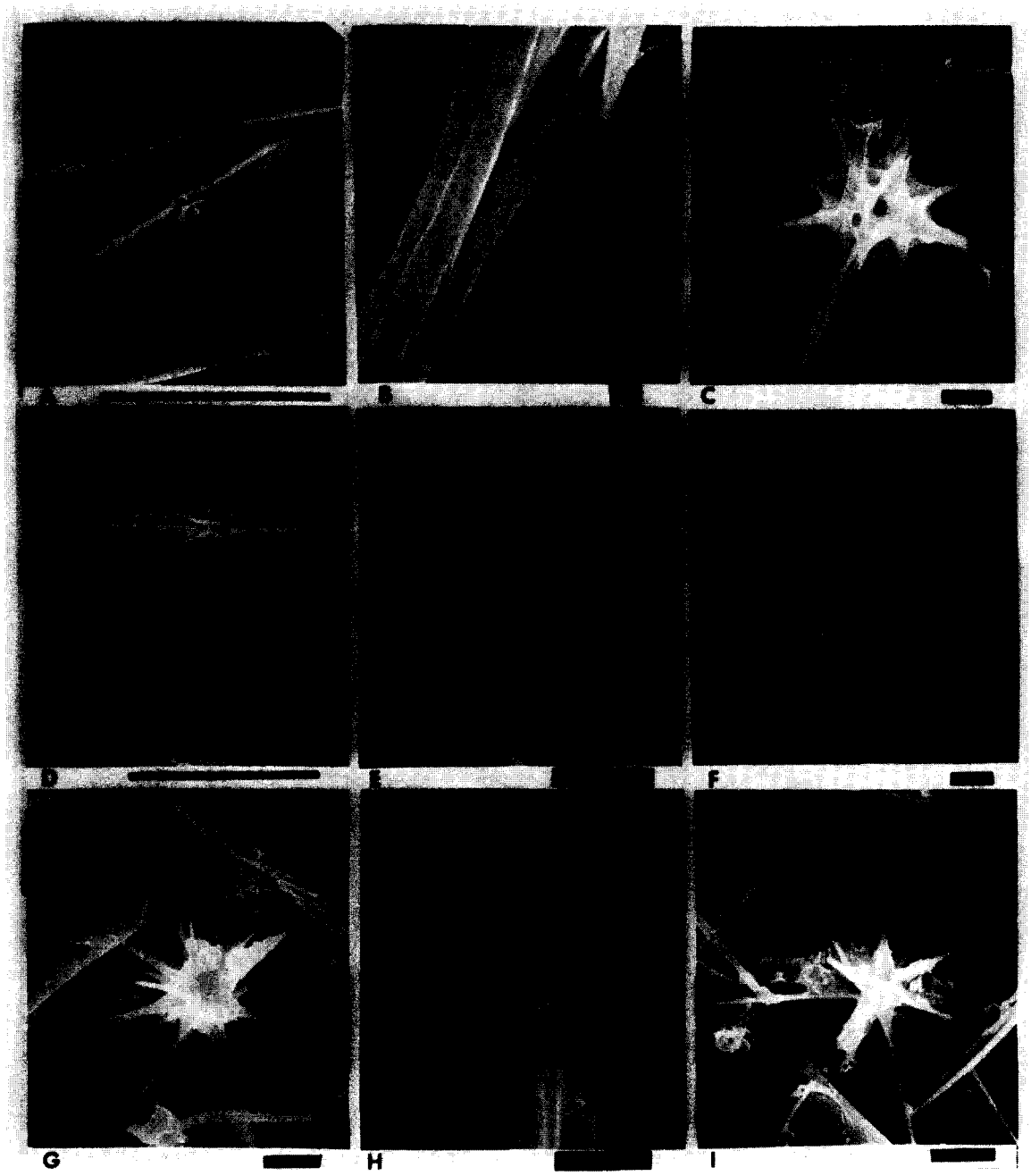

Fig. 10. Scanning electron micrographs of Acantharia on 53-μm filters from 32, 50, and 113 m showing effects of dissolution. Scale indication: ■ 1 μm, ■ 10 μm, ■ 100 μm. A. Acantharian of the genus *Amphibelone*, 32 m. B. Enlargement of lower middle spicule of C. Note membranous coating and well-defined edges of the spine, 32 m. C. Polar view of *Tetralonche* sp. Haeckel. Upper portion is thickly coated with mucoid material, 32 m. D. *Amphibelone* sp., similar to A and portions of Radiolarian inner capsule, 50 m. E. Enlargement of upper left spine, F, 50 m. F. Equatorial view of *Tetralonche* sp., 50 m. G. Remains of *Tetralonche* sp. and portions of two centrate diatoms, *Coscinodiscus* sp. and *Bacteriastrum* sp., 113 m. H. Enlargement of I. Note: dissolution causes fine structure to appear at edges of spicule in comparison to B, 113 m. I. *Astrolithium* sp., heavily coated with debris, 113 m.

(facing p. 534)

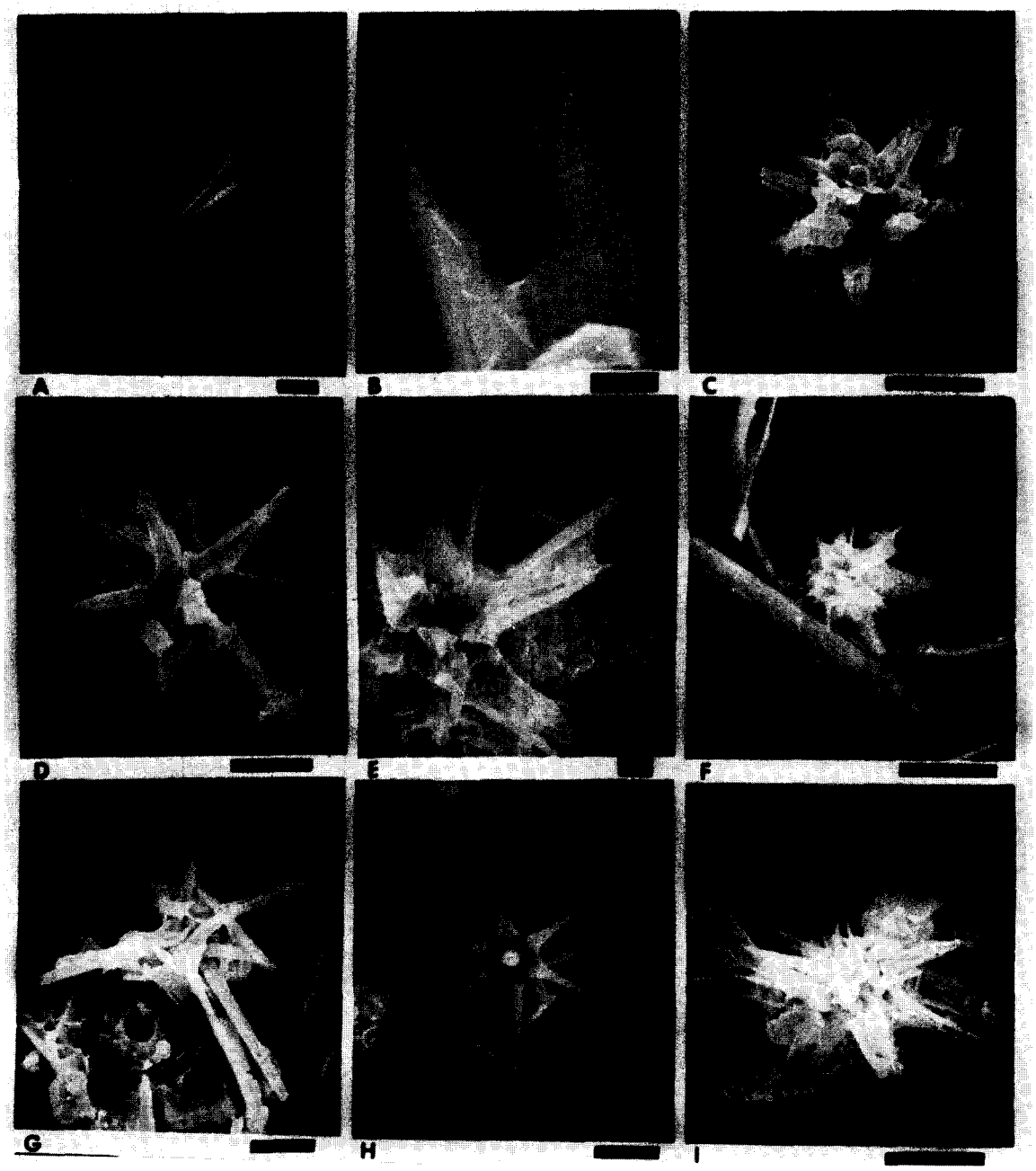

Fig. 11. Scanning electron micrographs of Acantharia on 53-μm filters from 188, 294, and 388 m showing effects of dissolution. Scale indication is the same as for Fig. 10. A. *Acantholithium* sp., with equal length, radially arranged spicules, 188 m. B. Enlargement of C, spicule exhibits double point structure as a result of etching, 188 m. C. Acantharian that has lost primary features of spicules by dissolution and fragmentation. Central area is obscured by tests and debris, 118 m. D. Partially dissolved acantharian of the family Stauracanthidae. Note additional orthogonal spines on major spicules, 294 m. E. Enlargement of F, showing well-developed double point structure arising from dissolution, 294 m. F. Acantharian with associated organic debris. Remains of a centrate diatom frustule are in the background, 294 m. G. Remaining structure of acantharian with non-articulating spicules; probably a member of the family Acanthochiasmidea. Sections of protozoan tests are below the acantharian, 294 m. H. Well-preserved *Astrolithium bulbiferum*, 388 m. I. Largely dissolved acantharian with debris in background, 388 m.

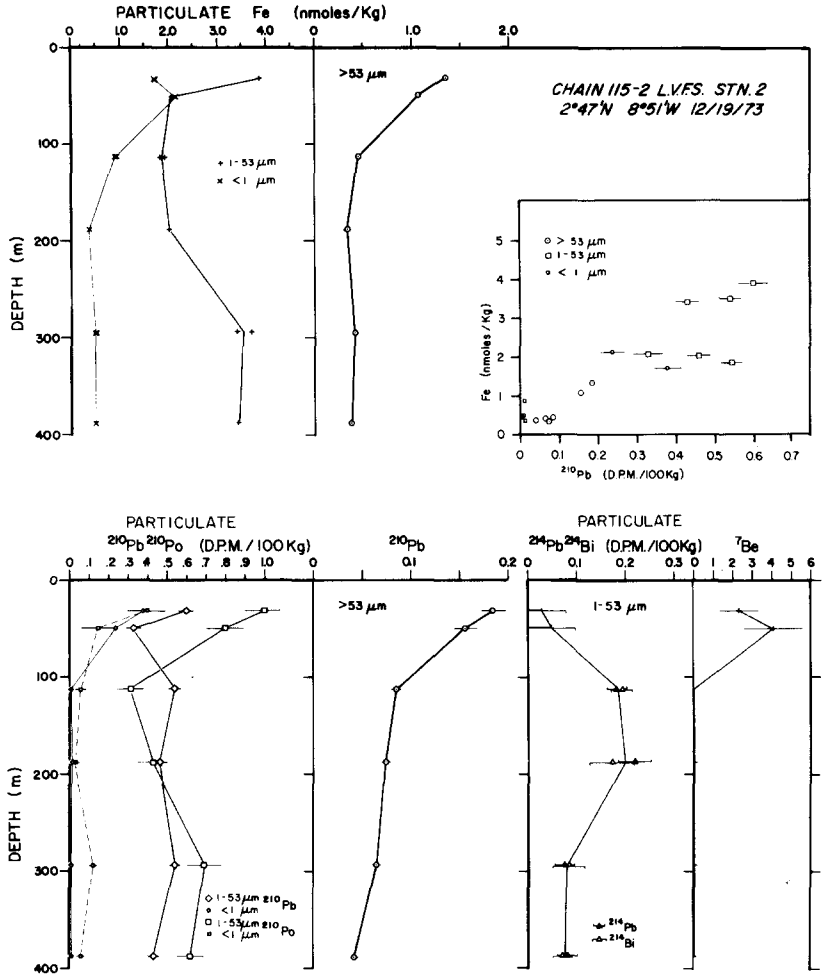

Fig. 12. Upper: particulate iron showing strong correlation with ^{210}Pb. Lower: particulate ^{210}Pb and ^{210}Po, ^{214}Pb and ^{214}Bi, and ^{7}Be, activities in the three size fractions. ^{214}Pb and ^{214}Bi activities are equivalent to the ^{226}Ra activity. ^{7}Be and ^{226}Ra were undetectable in the > 53-μm size fraction.

settling rates for the particles in each size fraction and hence allow independent calculation of vertical fluxes.

Results for ^{210}Pb and ^{210}Po are shown in Fig. 12 and summarized in Table 10. It was not possible to analyze the > 53-μm samples soon enough to determine ^{210}Po; only ^{210}Pb data are available for this size fraction.

Maximum particulate ^{210}Pb activities were at 32 m in all size fractions. The only other element showing a surface maximum is iron and the two elements covary (Fig. 12). Because the principal source of ^{210}Pb in the upper part of the water column is delivery from the atmosphere, the similarity between the two distributions (note especially the > 53-μm size fraction) may indicate an atmospheric source for particulate iron.

The particulate ^{210}Po maximum at 32 m does not reflect the atmospheric source (^{210}Po/^{210}Pb activity ratio in air and rain water samples is approximately 0.1; BURTON and STEWART, 1960; LAMBERT and NETAMI, 1965; POET, MOORE and MARTELL, 1972) but

is due to the rapid uptake of this nuclide from seawater. The greatest enrichment of ^{210}Po is found at 50 m, the particle maximum, where the ^{210}Po/^{210}Pb activity ratio is 2.4. This value of relative enrichment is within the reported range for phytoplankton (SHANNON, CHERRY and ORREN, 1970). It is interesting to note, however, that ^{210}Po and ^{210}Pb are more highly concentrated in particulate matter than in plankton (Table 11). In the < 1-μm size fraction ^{210}Pb is essentially absent below 50 m, unlike ^{210}Po which is readily measurable below this depth. Such behavior is consistent with the known behavior of the Pb and Po isotopes; ^{210}Po is readily adsorbed onto surfaces and should be enriched in the smallest particle size fraction (^{210}Po blank levels were insignificant for glass fiber filters exposed to seawater for several hours).

Table 11. ^{210}Lead and ^{210}Polonium contents of particulate matter compared with those of plankton. Units: dpm g^{-1} dry wt. Total range reported is given along with medians (in parentheses).

	Pb - 210	Po - 210
CHAIN 115-2 LVFS Stn. 2		
particulates : < 1 μm	60-710 (85)	190-1090 (310)
1-53 μm	100-430 (320)	170- 560 (350)
> 53 μm	62-610 (215)	n.d.
Phytoplankton*	0.5-3.1 (0.9)	1.9-7.3 (4.8)
Zooplankton*	0.4-2.8 (1.0)	10.0-30.9 (13.)
Zooplankton†	0.2-6.1 (1.4)	2.2-196. (30.)

* Based on SHANNON, CHERRY and ORREN (1970); assumed wet to dry weight ratio = 20.
† TUREKIAN, KHARKAR and THOMSON (1974).

Particulate ^{210}Po activity passes through a well-developed minimum at 113 and 188 m, where the ^{210}Pb/^{210}Po activity ratios are less than 1.0. This behavior is consistent with the conclusion of BACON (1975) that ^{210}Po is rapidly recycled within the thermocline, where the ^{210}Po/^{210}Pb activity ratios in filtered seawater frequently exceed 1.0. These data also indicate that ^{210}Po and ^{210}Pb exist in separate particulate phases in the shallow samples.

^{7}Be ($t_{1/2}$ = 53 day) has a stratospheric origin and is probably introduced at the sea surface by wet deposition (SILKER, 1972). Both the 1- to 53-μm and > 53-μm fractions were analyzed but the only measurable activities were at 32 and 50 m in the 1- to 53-μm fraction. The correlation with organic carbon [4×10^4 dpm(mole C)$^{-1}$, and 6×10^4 dpm (mole C)$^{-1}$ at 32 and 50 m, respectively] may be a phenomenon of surface adsorption rather than active uptake since the > 53-μm fraction exhibited no measurable ^{7}Be activity at 50 m.

^{226}Ra *as determined by* ^{214}Pb *and* ^{214}Bi

A by-product of the ^{7}Be analyses was that measurable activities of ^{214}Pb ($t_{1/2}$ = 26.8 min) and ^{214}Bi ($t_{1/2}$ = 19.7 min) were found in the 1- to 53-μm samples; no measurable activity was found in the > 53-μm samples. These isotopes are short-lived daughters of ^{226}Ra ($t_{1/2}$ = 1622 yr); assuming no loss of ^{222}Rn ($t_{1/2}$ = 3.82 day), the activities of ^{214}Pb and ^{214}Bi are equivalent to that of ^{226}Ra. ^{226}Ra is important in that it is an independent radioactive tracer of oceanic circulation, having different sources than ^{14}C. An understanding of the particulate ^{226}Ra distribution and fluxes in the ocean is necessary to provide sufficient constraints on the rates of regeneration of particulate ^{226}Ra in the water column, and hence allow its use as a time tracer of oceanic circulation.

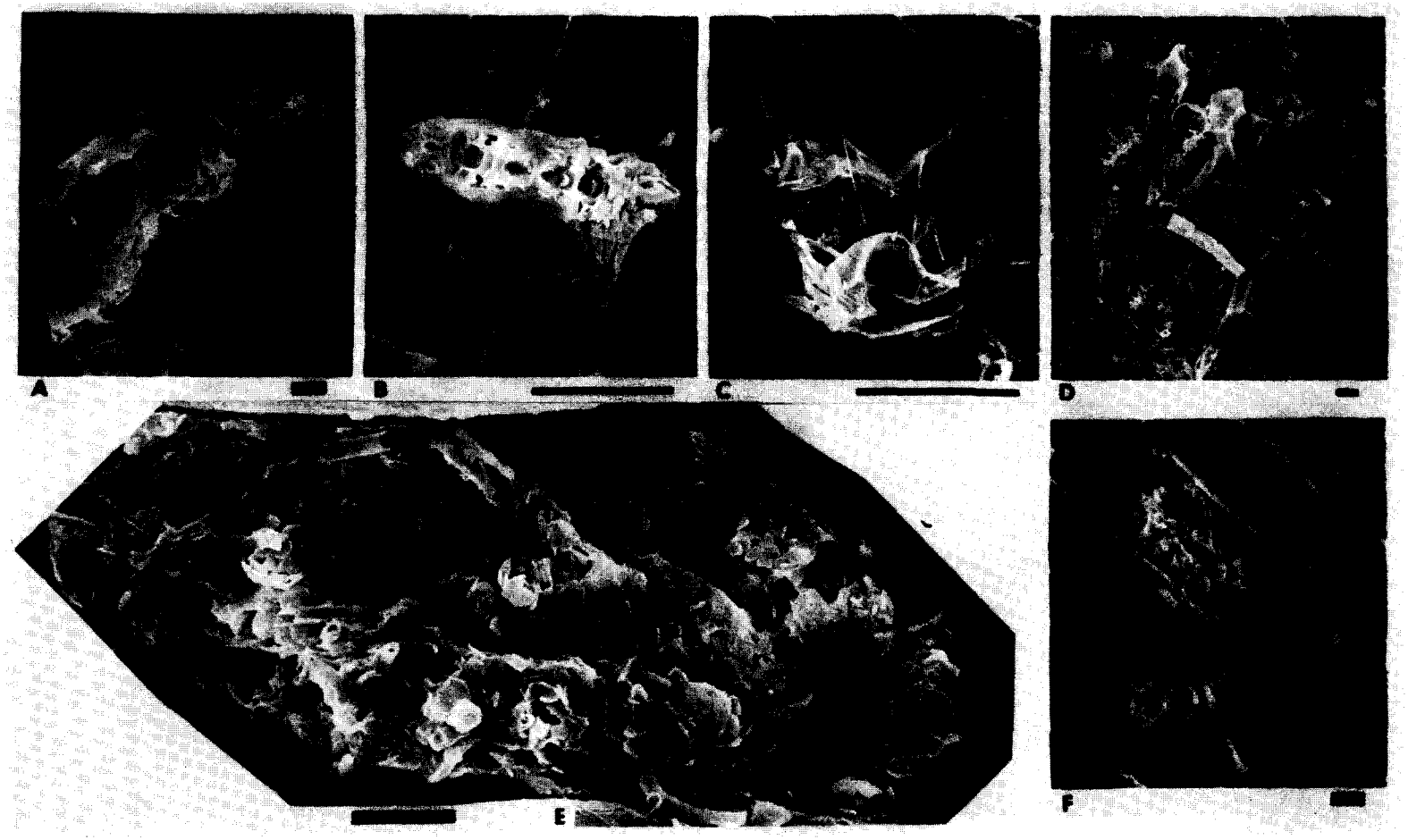

Fig. 13. Scanning electron micrographs of biogenic debris on 53-μm filters from various depths. Scale indication is the same as for Fig. 10. A. Remains of a crustacean carapace discarded during a molt, 388 m. B. Central view of abdominal segments and appendages of a copepod exoskeleton; valvar view of diatom *Asteromphalus* sp, 113 m. C. Folded, membranous material from a crustacean carapace, 113 m. D. Portions of crustacean opal and thoracic appendages, 113 m. E. Magnification of F, typical fecal pellet incorporating coccoliths, intact coccolithophorids, diatom frustules, and organic materials, 113 m. F. Typical fecal pellet, 113 m.

(facing p. 536)

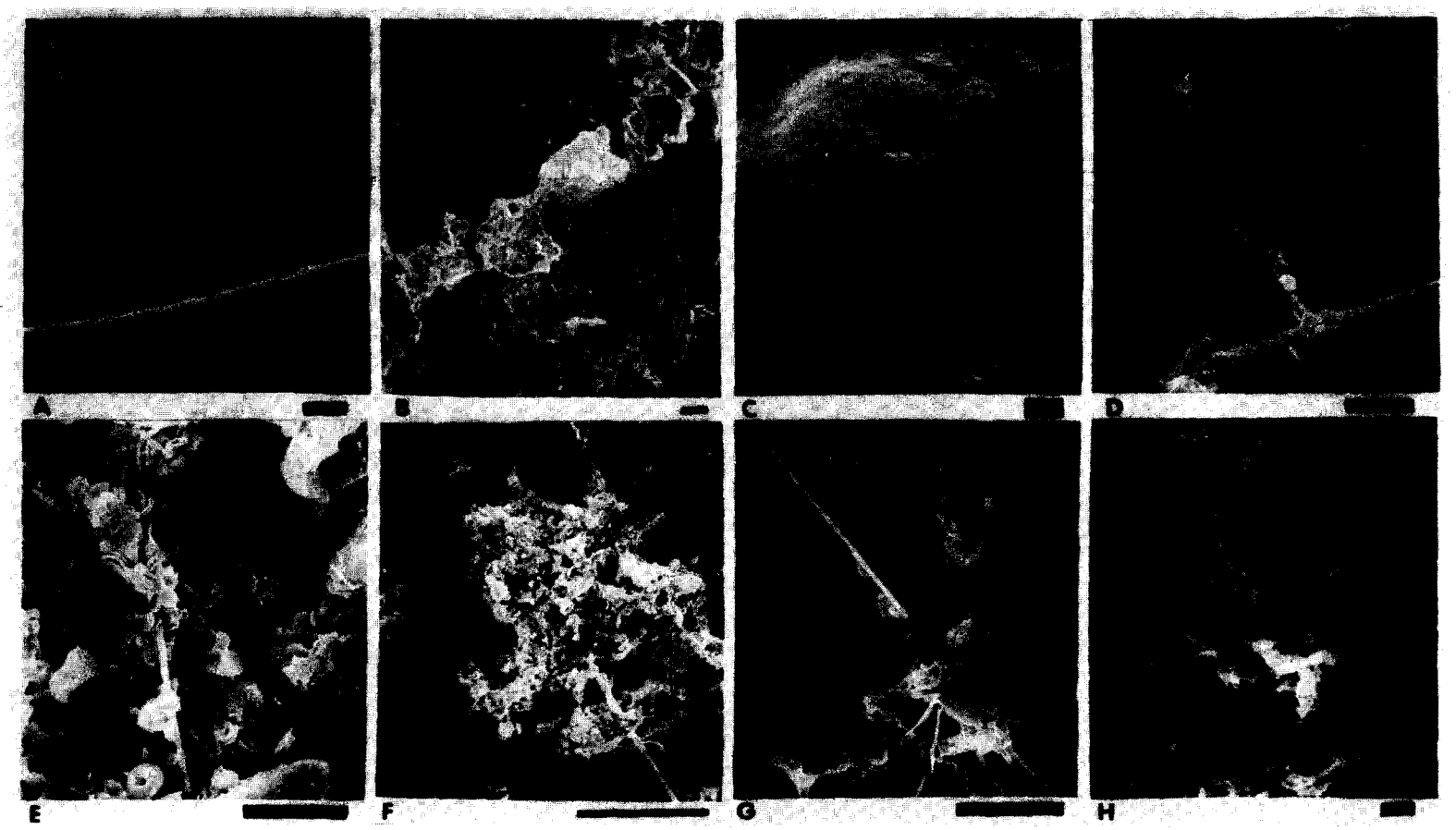

Fig. 14. Scanning electron micrographs of biogenic material on 53-μm filters from various depths. Scale indication is the same as for Fig. 10. A. Mucoid web-like organic material held in the 53-μm grid of the prefilter, 32 m. B. Hyaline-sheetlike particle, 50 m. C. Magnification of B, surface of this material is completely devoid of small particles such as coccoliths, 50 m. D. Fecal matter containing fragments of Acantharia, 388 m. E. Magnification of F showing contents of fecal matter. Contains a diversity of coccoliths and diatom and protozoan fragments, 388 m. F. Typical fecal matter, 388 m. G. Magnification of H, fecal matter containing Acantharian spine, fragmented tests and frustules, as well as organic material, 388 m. H. Fecal matter, 388 m.

The shapes of the ^{214}Pb and ^{214}Bi profiles closely resemble those of calcium carbonate and opal. The inferred ^{226}Ra distribution is unlike that of Sr* or total organic C, N, and P, suggesting that the bulk of the ^{226}Ra is fixed in the hard parts of the plankton growing above 100 m. Maximum values of $^{226}Ra/CaCO_3$ and $^{226}Ra/Si$ are calculated to be $6.5 \times 10^{-11} \pm 2.5 \times 10^{-11}(\sigma)$ and $2.0 \times 10^{-10} \pm 1.3 \times 10^{-10}(\sigma)$, respectively. Some ^{226}Ra may be associated with a refractory component of organic matter like excess Mg or Ca. The application of vertical advection-diffusion models to the dissolved distribution of ^{226}Ra, alkalinity, and silicate in the deep tropical Pacific gives an average *in situ* production ratio of $^{226}Ra/CaCO_3 = 6 \times 10^{-11}$ and $^{226}Ra/Si = 5 \times 10^{-11}$ (CHUNG and CRAIG, 1973; EDMOND, 1974). These similar estimates are uncertain because the calculated rates of regeneration of carbonate and opal within the water column included zero at the 95% confidence limit (2σ).

LARGE PARTICLES AND VERTICAL FLUXES

Large aggregate particles, particularly fecal pellets, have been suggested as important in the sedimentation of clay minerals, coccoliths, coccospheres, diatoms (BRAMLETTE, 1961; GOLDBERG and GRIFFIN, 1964; BISCAYE, 1965; CALVERT, 1966; SCHRADER, 1971; MANHEIM, HATHAWAY and UCHUPI, 1972; LISITZIN, 1972; HONJO, 1975; ROTH, MULLIN and BERGER, 1975), and carbon (MENZEL, 1974). The state of preservation and distribution of coccoliths and the distribution of clay minerals in sediments can only be explained in terms of rapid vertical transport of these small particles to the sediments with little or no interaction with the water column. The occurrence of bottom dwelling organisms below zones of high surface biological productivity (HEEZEN and HOLLISTER, 1971) must also reflect increased transport of organic carbon to the sediments in these areas. Model calculations such as those by MCCAVE (1975) showed that large particles such as fecal pellets would be rare in the water column and hence would be missed by conventional techniques used to sample particulate matter in the water column. BISHOP and EDMOND (1976) have shown this to be true for waters shallower than 400 m. The LVFS sampling was designed to test the hypothesis of 'fecal pellet' sedimentation.

Figures 13 and 14 show the morphology of large single and composite organic particles. These particles fall into the classifications: crustacean appendage and carapace material (Fig. 13A to D); mucoid material (Fig. 14A); hyaline sheet-like material (Fig. 14B and C); fecal pellets (Fig. 13 E and F); and fecal matter (Fig. 14 D to H). The distinguishing feature of both the fecal pellets and fecal matter is that they contain coccospheres, coccoliths, whole and fragmented diatom frustules, small organic particles, as well as fragments of Foraminifera, Radiolaria, and Acantharia. The fecal pellets are generally cylindrically shaped and well aggregated; the fecal matter less so. Smaller particles in these classes have probably been recognized by GORDON (1970) and RILEY (1970).

Figure 15 shows the profiles of carbonate/Foraminifera, silicate/Radiolaria, silicate/diatom, and Sr*/Acantharia in the > 53-μm size fraction (whole tests and frustules only). The carbonate/Foraminifera profile shows an order-of-magnitude increase with depth indicating the enrichment of the > 53-μm fraction with coccoliths and other carbonate fragments. Silicate/Radiolaria or diatom profiles are non-variant; the values are much higher than those calculated for Radiolaria and diatoms in the LVFS samples. Sr*/Acantharia increases by a factor of 5 down to 188 m and then suddenly drops back to near-surface values deeper. These observations are consistent with SEM studies of the large particles, which showed them to become progressively enriched in fragments

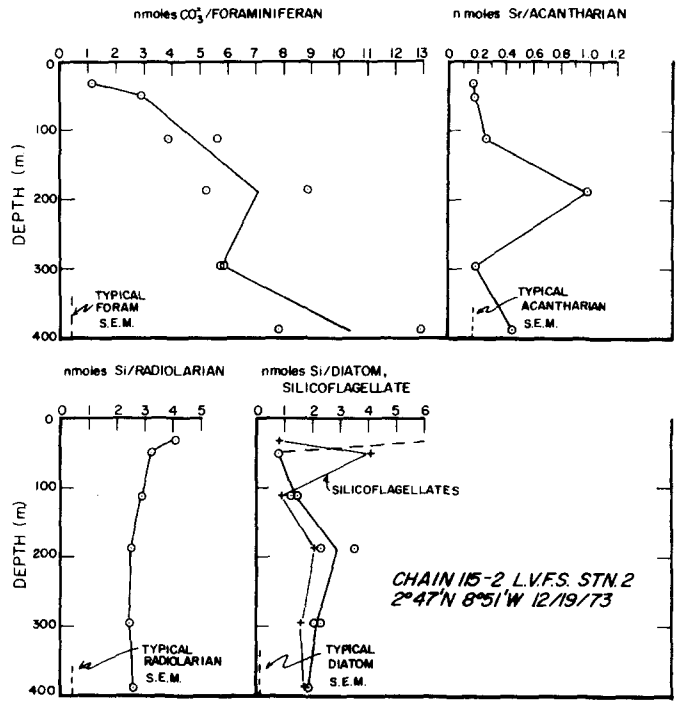

Fig. 15. Carbonate per Foraminifera, silicate per Radiolaria and per diatom, non-carbonate strontium per Acantharia, ratios in the >53-μm size fraction indicate that the contribution of *whole* organisms to total carbonate, opal, and celestite is small at 388 m.

(coccoliths, broken diatoms, broken Radiolaria, and Acantharia spines) with increasing depth and also showed loss of $SrSO_4$ below 200 m because of dissolution.

A quantative light microscopic and SEM study of the size distribution and morphology of the large particles sampled at 388 m was made to calculate the vertical fluxes of mass, organic carbon, silicate, and carbonate through 388 m.

Figure 16 shows the size distribution of Foraminifera (dark and light grey bars) and foraminiferan fragments (light gray and white bars) determined by scanning approximately 1/50th of the 53-μm prefilter area of the 388 m sample. SEM measurements of broken Foraminifera were used to calculate a dry weight density of $0.5\,g\,cm^{-3}$ (total volume of calcite walls $\times\ \rho_{calcite} \div$ spherical volume, radius d = maximum dimension) based upon their geometry and 1-μm wall thickness. The size distribution data together with the calculated dry weight density shows that whole Foraminifera contribute $0.20\,nmoles\,kg^{-1}$ of seawater or 6% to the total suspended carbonate concentration in the >53-μm fraction. The size distribution, typical shapes, and thicknesses of the foraminiferan fragments show that they account for only 1% of the total carbonate on the 53-μm filter. Approximately 93% of the >53-μm carbonate, largely coccoliths, is bound in aggregate particles.

The contribution of whole and fragmented Radiolaria, diatoms, and silicoflagellates to total silica in the >53-μm fraction is harder to estimate. MOORE (1969) showed that the average Radiolaria (estimated size, 100 μm) in recent sediments from the tropical Atlantic weighed 0.05 μg or contained 0.7 nmole Si (assuming opal contains 15% water; MOORE,

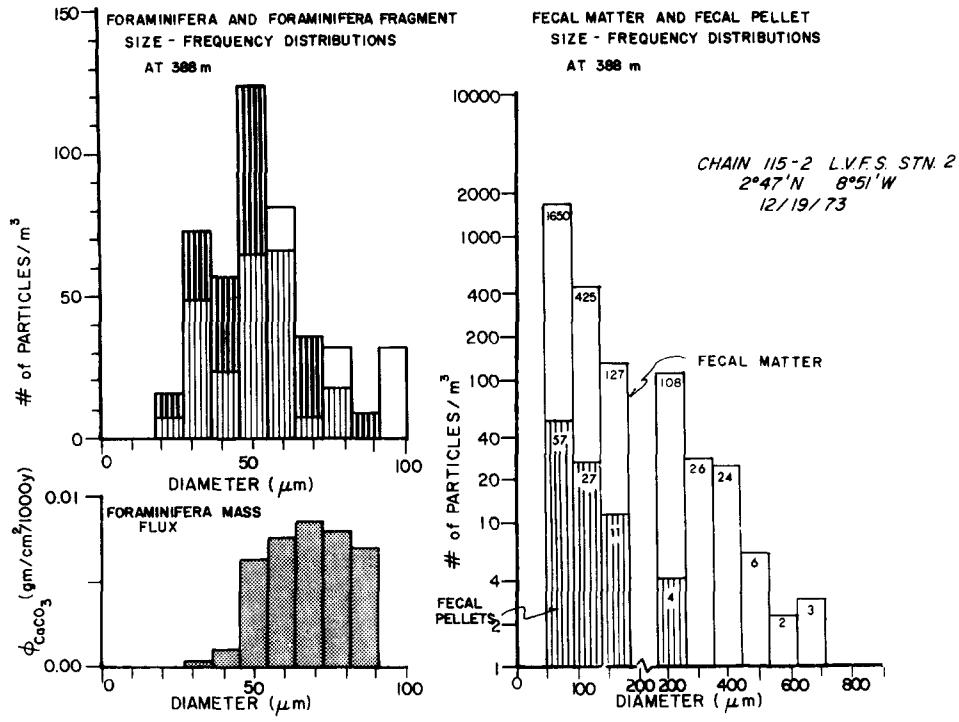

Fig. 16. Left: upper, size frequency distribution of Foraminifera (dark and light grey bars) and Foraminifera fragments (white and light grey bars) per cubic meter based on 442-l. subsample; lower, carbonate mass flux through 388 m carried by Foraminifera. Right: size–frequency distribution of fecal matter and fecal pellets contained in 1 m^3 based on a 442-l. subsample; the >300-μm particles were counted on a filter subsample equivalent to 1045 l.

1969). A typical (70 μm) radiolarian at 388 m at this station is estimated to contain 0.4 nmole Si. Similarly, the average 60-μm diatom accounts for 0.11 nmole Si and the largest (40 μm) silicoflagellate would contain 0.012 nmole Si. The total silicon in whole organisms may account for 22% of the total present on the 53-μm filter. Separate fragments are estimated to account for an additional 3% of the total silica. Thus 75% of the total silica is composed of diatom and radiolarian fragments within the fecal material.

The mole ratio of carbonate to silicate in the large aggregate particles is 0.90 at 388 m (from Table 9 and the above discussion). These particles are calculated to be 60% organic matter by weight (CH_2O+N) from a comparison of the dry weights of the particles removed from the 53-μm filter with the results of C and N analyses of this material (Table 6). Thus, organic carbon, calcium carbonate, and opal make up 24, 22.5, and 17.5%, respectively, of the dry weight of fecal pellets and fecal matter.

Large particle flux through 388 m

STOKES' (1901) law is used to calculate the particulate flux.

$$v_d = \frac{g}{18\eta}\Delta\rho d^2 \qquad \text{cm s}^{-1}. \tag{2}$$

v_d is the particle settling velocity; η, the water viscosity, is 0.0145 poise at 388 m; d is

the diameter of the particle; g is the gravitational acceleration; $\Delta\rho$ is the density contrast of the particle with seawater,

$$v_d = 3.75 \times 10^3 \Delta\rho d^2 \qquad \text{cm s}^{-1}. \tag{3}$$

The mass flux, Φ_d is:

$$\Phi_d = m_d v_d \qquad \text{g cm}^{-2}\,\text{s}^{-1} \tag{4}$$

$$= n_d \frac{\Pi}{6} d^3 \rho_p v_d, \tag{5}$$

where n_d is the number of particles of size d per ml of seawater; ρ_p is the dry weight density of the particles, and m_d is the suspended mass concentration of particles of size d. Thus:

$$\Phi_d = 1.96 \times 10^3 n_d \Delta\rho \rho_p d^5. \tag{6}$$

Naturally occurring particles are neither spherical nor do they have smooth surfaces. This is taken into account by actually measuring the settling velocities of particles and calculating the density contrast of the particles with the seawater, $\Delta\rho'$, if they fell according to Stokes' law. This approach is rather circular, but it does allow us to draw on literature describing the settling behavior of these particles to calculate vertical fluxes. ρ_p is the dry weight of the particle divided by volume of a sphere of diameter d. It is assumed constant for a given particle type.

Thus:

$$\Phi_d = 1.96 \times 10^3 n_d \Delta\rho' \rho_p d^5 \qquad \text{g cm}^{-2}\,\text{s}^{-1} \tag{7}$$

or

$$\Phi_d = 6 \times 10^{13} n_d \Delta\rho' \rho_p d^5 \qquad \text{g cm}^{-2}(1000\,\text{yr})^{-1} \tag{8}$$

in sedimentary units.

The vertical fluxes of mass, carbonate, opal, and organic carbon may be calculated for this material using measurements of d, n_d, and chemical composition, which can be precisely determined. ρ_p and $\Delta\rho'$ can be obtained from the literature or estimated by SEM.

Flux of foraminiferan tests

The lower portion of Fig. 16 illustrates the carbonate flux-size distribution for the Foraminifera at 388 m. For the mass flux calculations, $\rho_p = 0.5\,\text{g cm}^{-3}$ and $\Delta\rho' = 0.3\,\text{g cm}^{-3}$ (BERGER and PIPER, 1972); the total flux is 0.22 mmole (0.02 g) $CaCO_3$ cm^{-2} (1000 yr)$^{-1}$ and is carried by Foraminifera larger than 50 μm (see Fig. 16). No Foraminifera larger than 100 μm were encountered on the subsample studied (equivalent to 440 l of seawater) even though typical foraminiferal ooze contains tests up to several hundred micrometers in diameter. Foraminifera 180 μm in size were encountered on subsamples of shallower filters. Their absence from the 388-m sample coupled with the presence of large (100-μm) fragments suggests that the > 100-μm Foraminifera concentration has been lowered to less than 1 m^{-3} at 388 m by grazing organisms. The number of large Foraminifera at this depth is consistent with the results of BERGER (1968).

The radiolarian silica flux is calculated to be 0.23 mmole Si (0.016 g opal (cm^{-2} (1000 yr)$^{-1}$ using the values $d = 70$ μm, $\rho_p = 0.1\,\text{g cm}^{-3}$ (MOORE, 1969), $\Delta\rho' = 0.1\,\text{g cm}^{-3}$ (assumed), and $n_d = 1.6 \times 10^{-3}$ (Table 5); the diatom and silicoflagellate fluxes are negligible.

Fecal matter and pellet fluxes

The right-hand side of Fig. 16 shows the size distributions of both fecal matter and fecal pellets based on a filter subsample equivalent to 440 l. of seawater at 388 m; in the case of the fecal matter distributions, the particles > 300 μm were counted on a filter area equivalent to 1050 l of seawater. The data (plotted on a vertical log scale) shows that fecal pellets are rare compared to the fecal matter. The dry weight density, ρ_p, of a fecal pellet is estimated to be approximately 0.5 g cm^{-3} (WIEBE, BOYD and WINGET, 1976; HONJO, 1976). The value for $\Delta\rho'$ is assumed to be 0.2 g cm^{-3} (range 0.1 to 0.5 g cm^{-3}) based on data from SMAYDA (1971) and FOWLER and SMALL (1972). Both ρ_p and $\Delta\rho'$ are calculated based on d = maximum pellet dimension. The fecal matter is *assumed* to have a dry weight density of 0.2 g cm^{-3} (these particles are less densely packed than pellets), and $\Delta\rho' = 0.05$ (they are irregularly shaped). The fecal matter dimension, d, is the average of length and width; the ratio of length to width of this material ranged from 1 to 5 with 87% of the particles having a ratio of 2.

Table 12. Mass and element fluxes of fecal pellets through 388 m.

$dx10^4$ (μm)**	$n_d x10^3$ (#/ℓ)	$m_d x10^9$ (μg/ℓ)	Φ_m	$\Phi_{C_{org}}$	Φ_{CaCO_3}	Φ_{opal}
			(gm/cm^2/1000y)			
46	0.057	0.001	0.0007	0.0002	0.0002	0.0001
91	0.027	0.005	0.010	0.002	0.002	0.002
137	0.011	0.007	0.032	0.008	0.007	0.006
183	0.004	0.006	0.049	0.012	0.011	0.009
TOTAL FECAL PELLET FLUX			0.091	0.022	0.021	0.016

* Based on count of filter area equivalent to 440 l.
** Maximum length of pellet, length to width ratio averages 3.

Table 13. Mass and element fluxes of fecal matter through 388 m.

$dx10^4$ (μm)††	$n_d x10^3$ (#/ℓ)	$m_d x10^9$ (μg/ℓ)	Φ_{mass}	$\Phi_{C_{org}}$	Φ_{CaCO_3}	Φ_{opal}
			(gm/cm^2/1000y)			
47	1.650	0.016	0.002	0.000	0.000	0.000
91	0.425	0.034	0.016	0.004	0.004	0.003
137	0.127	0.034	0.037	0.009	0.008	0.006
183	0.108	0.069	0.132	0.032	0.030	0.023
274	0.026	0.056	0.240	0.058	0.054	0.042
365	0.024	0.122	0.935	0.225	0.210	0.164
457	0.006	0.060	0.714	0.171	0.161	0.125
548	0.002	0.034	0.592	0.142	0.133	0.104
639	0.003	0.082	1.919	0.461	0.432	0.336
TOTAL FECAL MATTER FLUX			4.590	1.102	1.033	0.803

† Based on count of filter area equivalent to 440 J: for > 300-μm particles the filter area corresponded to 1045 l.
†† d is the average dimension = $(l+w)/2$; l/w ranges from 1 to 5, averages 2.

The flux calculations are summarized in Tables 12, 13, and 14, which show that fecal matter and fecal pellets account for 99% of the mass flux through 388 m. The fluxes are: 94 mmole (1.10 g) $C_{org}\,cm^{-2}\,(1000\,yr)^{-1}$; 10.8 mmole (1.08 g) $CaCO_3\,cm^{-2}\,(1000\,yr)^{-1}$, mainly coccoliths; and 12.1 mmole Si (0.85 g opal) $cm^{-2}\,(1000\,yr)^{-1}$, mainly diatom fragments. For comparison, LISITZIN (1972) reported Holocene mass sedimentation rates of between 1.8 and 4.5 $g\,cm^{-2}(1000\,yr)^{-1}$; as this material is mainly carbonate and opal, the rate reported is in agreement with the calculated flux. EDMOND (1974) suggested that carbonate and opal are rapidly sedimented and that the transport of these different chemical species by a common carrier (e.g. fecal matter) explains the 2:1 correlation of alkalinity with silicate in seawater over much of the world's oceans.

Comparison of the organic carbon flux through 388 m, 94 mmole $C\,cm^{-2}\,(1000\,yr)^{-1}$, with the carbon productivity of these waters, 750 to 1500 mmole $C\,cm^{-2}\,(1000\,yr)^{-1}$ (UN–FAO, 1972) suggests that at least 87% of the organic carbon, 91% of the nitrogen, and 94% of the phosphorus fixed by photosynthesis in the surface waters has been recycled above 388 m. If the remaining carbon reaches the ocean floor and is consumed by bottom dwelling organisms, the resultant oxygen consumption would be 94 mmole $O_2\,cm^{-2}\,(1000\,yr)^{-1}$ (2.4 ml O_2 at S.T.P. $m^{-2}\,h^{-1}$) and compares with *in situ* bottom

Table 14. Flux summary for $>53\,\mu m$ particles at 388 m.

Particle	Φ_{mass}	$\Phi_{C_{org}}$	Φ_{CaCO_3}	Φ_{opal}
		(gm/cm²/1000y)		
FECAL MATTER	4.59	1.102	1.033	0.803
FECAL PELLETS	0.091	0.022	0.021	0.016
FORAMINIFERA	0.022	-	0.022	-
RADIOLARIA	0.02	-	-	0.02
TOTAL MASS FLUX	4.72	1.124	1.076	0.845
TOTAL CHEMICAL* FLUX		93.5	10.8	12.1

* mmoles cm^{-2} 1000 yr^{-1}.

respirometer measurements of oxygen consumption of 20 mmoles $O_2\,cm^{-2}\,(1000\,yr)^{-1}$ (0.5 ml O_2 at S.T.P. $m^{-2}\,h^{-1}$; SMITH and TEAL, 1973) at 1850 m, 39°N, 70°W. More recent measurements by Smith were reported by WIEBE, BOYD and WINGET (1976) to be 117 mmoles $O_2\,cm^{-2}(1000\,yr)^{-1}$ (3.0 ml O_2 at S.T.P. $m^{-2}\,h^{-1}$) at 24°50'N, 77°40'W at 2000-m depth. The organic carbon flux through 388 m is therefore sufficient to satisfy the respiratory requirements of bottom-dwelling organisms.

It is of interest to calculate the particulate flux of ^{210}Pb through 388 m, which should approximate the delivery rate of atmospheric ^{210}Pb to the sea surface (BACON, 1975). At 388 m the ^{210}Pb activity of particles in the >53-μm size fraction is 0.38 dpm mg^{-1}. The mass flux of 4.7 mg $cm^{-2}\,yr^{-1}$ estimated above for this depth yields a ^{210}Pb flux of 1.8 dpm $cm^{-2}\,yr^{-1}$; a result in fair agreement with estimates of atmospheric ^{210}Pb delivery rates. BACON (1975) for example, estimated a flux of 0.6 dpm $cm^{-2}\,yr^{-1}$ for the tropical North Atlantic. This value was an average for a large oceanic region; a station, such as Chain 115 LVFS Sta. 2, close to the continental source, would be expected to receive

higher than average fluxes. In any case the result shows that the ^{210}Pb flux carried by particles larger than 53 μm is sufficient to maintain the ^{210}Pb material balance for the upper layers of the water column.

A further check on the model parameter, ρ_p, can be made by calculating the suspended mass and element concentrations due to the various categories of large particles (Table 15). The calculated mass and element concentrations are lower than those observed, consistent with the microscopic observation that many aggregate particles < 53 μm were present on the prefilter. The flux carried by these particles is insignificant [$0.07\,g\,cm^{-2}(1000\,yr)^{-1}$; $m_d = 0.7 \times 10^{-9}\,g\,cm^{-3}, d = 40\,\mu m, \Delta\rho' = 0.05\,g\,cm^{-3}$]. Thus the assumed fecal matter dry weight density is consistent with the data.

Table 15. Suspended particulate concentration–mass concentration summary: > 53 μm at 388 m.

Particle	C_{org}	$CaCO_3$	SiO_2	mass
		(nmoles/kg)		
FECAL MATTER	10.1	1.14	1.27	0.507
FECAL PELLETS	0.41	0.046	0.051	0.021
FORAMINIFERA	-	0.15	-	0.015
FORAMINIFERA FRAGMENTS		0.02	-	0.002
RADIOLARIA + FRAGMENTS	-	-	1.03	0.070
TOTAL	10.5	1.36	2.35	0.545
OBSERVED	15.9*	2.98	4.11	1.08*

* Result is probably low, > 53-μm C/P ratio is a factor of 2 lower than expected; see Table 6, Fig. 5, Estimate $C_0 \sim 25\,nmoles\,kg^{-1}$; [P.M.] = $1.5\,\mu g\,kg^{-1}$.

The above flux calculations are based on several assumptions about the sinking behavior of the material collected by the LVFS. We have tried to constrain the values of the model parameters where possible but some, particularly $\Delta\rho'$ of fecal matter, are based largely on SEM evidence. As a result the flux calculations are probably within a factor of 2 or 3 of the true value. It must be stressed that these calculations are based on samples collected over a period of 1 day from an area of the ocean of a few tens of square kilometers. Whether or not the particle flux changes with time remains to be determined.

One of the most important conclusions from this calculation is that the fecal material is important in sedimentation of small particles such as coccoliths; however, it appears that most of the mass flux is carried by *fecal matter* rather than fecal pellets as had been previously suggested. Furthermore, this material is capable of satisfying the respiratory requirements of the bottom-dwelling organisms found in association with areas of high surface productivity.

Flux of < 53-μm particles

An approximation of the sinking velocity of the 1- to 53-μm particles can be made using the ^7Be data, assuming that ^7Be remains associated with its particulate carrier; i.e. organic carbon. The ^7Be activity at 50 m divided by that at 113 m (normalized to C_{org}) is > 32, corresponding to a ^7Be decay over a time interval of at least 5 half-lives

(265 days). The particle settling velocity is $< 3 \times 10^{-4}$ cm s^{-1}, corresponding to a Stokes' Law particle diameter of 5 μm ($\Delta\rho' = 0.2$ g cm^{-3}). The mass flux, < 0.1 g cm^{-2} (1000 yr)$^{-1}$, is less than 2% of the total mass flux carried by the > 53-μm particles. The main assumption that ^{7}Be and its carrier are not fractionated by degradative processes in this depth interval may be violated. ^{7}Be might be rapidly lost from particles as in the case of ^{210}Po. Diffusive fluxes are likely to be negligible (RILEY, 1970; MCCAVE, 1975).

SUMMARY AND CONCLUSIONS

The samples of particulate matter collected at this station have been analyzed for the major biogenic chemical elements, δ^{13}C, iron, and radioisotopes ^{210}Pb, ^{210}Po, ^{7}Be, ^{214}Pb, and ^{214}Bi. Microscopic analyses have been made to determine the size and morphologic distributions of the particles to understand the mechanisms important in controlling the vertical distributions and fluxes of particles within the upper 400 m.

(1) A particle maximum occurs in the upper thermocline at 50 m and is associated with the plankton maximum. Sharp vertical concentration gradients between 50 and 113 m of particulate mass, whole organisms, and organic carbon, nitrogen and phosphorous are probably maintained by the action of filter feeding organisms.

(2) C/N and C/P ratios in the organic particles are a function of size and depth; the ratios are lowest in the < 1-μm size fraction and highest in the > 53-μm size fraction. The occurrence of bacteria and the grazing activities of zooplankton may account for this size-dependent behavior.

(3) The δ^{13}C distributions bear little resemblance to those of particulate C, N, and P. The presence of bacteria (being isotopically light, $\delta^{13}C = -36$‰) at 50 m may explain the 4‰ depletion of ^{13}C between 32 and 50 m observed for the < 1-μm and 1- to 53-μm size fractions. The > 53-μm particles behave consistently with the results of other workers; however, the probable presence of bacteria in all size fractions complicates the use of $^{13}C/^{12}C$ ratios of the organic carbon as an indicator of its composition.

(4) Eighty to 100% of the particulate calcium is balanced by carbonate. The remaining 'excess' calcium is probably a component of organism cytoplasm at 32 and 50 m and bound by ion-exchange in the 1- to 53-μm size fraction deeper in the water column. Ion-exchange capacity of the 1- to 53-μm particles at 294 m was measured to be 96 mequiv (100 g)$^{-1}$ (dry weight).

(5) Particulate magnesium is not ion-exchangeable nor is it in carbonate or phosphate phases. It is readily released from the particles on exposure to 10^{-3} N HCl and is probably strongly bound to a refractory component of the organic matter. Mg/C_{org} increases from 0.4 to 2 mole% down the water column to 400 m.

(6) Particulate organic matter is progressively enriched in cations with increasing depth to the extent that bound cation charge equals the nitrogen content of the particles at 294 m. The major anomalies in the calcium and alkalinity distributions postulated recently are probably restricted to the upper thermocline where most of the organic matter is recycled.

(7) Acantharia and their fragments comprise the bulk of the particulate Sr in the > 53-μm size fraction. Their dissolution progresses most rapidly below 188 m. Seventeen per cent of the total Sr is bound by ion exchange (like Ca) in the 1- to 53-μm particles at 294 m. In the upper 388 m some 50 to 75% of the > 53-μm Sr has been lost by dissolution of $SrSO_4$.

(8) Si and $CaCO_3$ distributions are controlled primarily by processes of fragmentation and aggregation within the upper 388 m. Small carbonate and opal particles are progressively enriched in the large particles with increasing depth.

(9) Particulate Fe and ^{210}Pb both exhibit a maximum at 32 m, consistent with an atmospheric source for both these elements.

(10) The greatest enrichment of ^{210}Po relative to ^{210}Pb was observed at 50 m, the organism maximum. ^{210}Po appears to exist in a separate phase from the ^{210}Pb and displays nutrient-like behavior as evidenced by its rapid depletion relative to ^{210}Pb between 50 and 113 m. ^{210}Po is most strongly enriched relative to ^{210}Pb on the < 1-μm particles below 50 m, consistent with its chemical behavior.

(11) ^{7}Be is correlated with organic carbon at 32 and 50 m. Decay of the ^{7}Be between 50 and 113 m allows an estimate of the sinking velocity of the < 53-μm organic particles over this depth interval of $< 3 \times 10^{-4}$ cm s^{-1}. The < 53-μm carbon flux is possibly 0.5 to 1.0 mmole C cm^{-2} (1000 yr)$^{-1}$, less than 1% of the large particle flux through 388 m.

(12) $^{226}Ra/CaCO_3$ and $^{226}Ra/Si$ mole ratios are 7×10^{-11} and 2×10^{-10}, respectively, in the 1- to 53-μm size fraction. The ^{226}Ra flux into the deep ocean is probably between 1.4 and 4.1×10^{-12} mole ^{226}Ra cm^{-2} (1000 yr)$^{-1}$ at this station; ^{226}Ra shows no correlation with total organic carbon or $SrSO_4$ in particles.

(13) From the flux calculations it is apparent that 87% of the organic carbon, 91% of the nitrogen, and 94% of the particulate phosphorus is recycled in the upper 400 m at this station. The elemental composition of the organic flux through 388 m is $C_{106}N_{11}Mg_{1.1}Ca_{0.2}P_{0.2}$. The carbon flux has a $\delta^{13}C$ value of -23.7‰ compared to the suspended carbon value of -21.2‰. The flux [94 mmole C cm^{-2} (1000 yr)$^{-1}$ is sufficient to meet the respiratory requirements of bottom dwelling organisms.

(14) The Fe, Mg, and Sr fluxes are 1.2, 0.9, and 0.15 mmole cm^{-2} (1000 yr)$^{-1}$. The Mg flux is such that it has no measurable effect on the dissolved Mg concentration.

(15) Flux calculations give values for carbonate (mainly coccoliths) and opal (mainly diatom fragments) deposition of 10.9 and 12.2 mmoles cm^{-2} (1000 yr)$^{-1}$ [1.09 and 0.85 g cm^{-2} (1000 yr)$^{-1}$], respectively, in agreement with observed sediment accumulation rates for carbonate. The flux ratio of carbonate and opal is consistent with the calculations by EDMOND (1974).

(16) The calculated ^{210}Pb flux (1.8 dpm cm^{-2} yr)$^{-1}$ is consistent with the results of BACON (1975).

(17) Transit times for the fecal material through the 4-km deep water column are estimated to be on the order of 10 to 15 days. The lateral displacement due to deep ocean advection, if unidirectional with depth (3 cm s^{-1}), would be between 26 and 39 km, indicating that the resulting sediment distributions would reflect oceanic variability of this scale.

(18) We observe that fecal material accounts for only 5% of the total particulate suspended mass concentration, but it accounts for over 99% of the vertical flux through 388 m.

All these points indicate that dramatic changes in the character of the particulate matter occur within the upper 400 m (particularly between 50 and 113 m at this station). Most of the particles are biogenic and their distribution and sedimentation are controlled primarily by biological processes within this depth interval. In addition to carbonate and opal carriers, organic matter has been shown to have ion-exchange and binding capacity and hence may be significant in minor and trace element fluxes in the ocean.

Acknowledgements—We would like to thank Captain PALMERI, COLLIN SUMMERHAYES (Chief Scientist), and the crew and scientific party of the R.V. *Chain* for their assistance in deploying the LVFS. AMY NG determined oxygen and nutrients; BOB STALLARD helped in the operation of the LVFS. PHIL CLARNER analyzed the samples for carbon and nitrogen. We would also like to thank Drs. SUSUMO HONJO, WERNER DEUSER, and PETER BREWER, who generously provided assistance as well as the use of their laboratory facilities at Woods Hole Oceanographic Institution. PAM THOMPSON drafted the figures. We have benefitted from discussions with Drs. DEREK SPENCER, FRED SAYLES, and MICHAEL BENDER as well as with ED BOYLE, BOB COLLIER and other members of the M.I.T. Geochemistry Collective. This work was supported at M.I.T. by the Office of Naval Research on contract N00014-75-C-0291; contribution number 12 from the Geochemistry Collective at M.I.T.

REFERENCES

BACON M. P. (1975) Applications of $^{210}Pb/^{226}Ra$ and $^{210}Po/^{210}Pb$ disequilibria in the study of marine geochemical processes, Ph.D. thesis, Massachusetts Institute of Technology–Woods Hole Oceanographic Institution, 165 pp.

BEAR F. E. (1964) *Chemistry of the soil*, Reinhold, 515 pp.

BERGER W. H. (1968) Planktonic foraminifera: shell production and preservation. Ph.D. thesis, University of California at San Diego, 241 pp.

BERGER W. H. and J. W. PIPER (1972) Planktonic Foraminifera: differential settling, dissolution, and redeposition. *Limnology and Oceanography*, **17**, 275–287.

BISCAYE P. E. (1965) Mineralogy and sedimentation of recent deep sea clay in the Atlantic Ocean and adjacent seas and oceans. *Bulletin of the Geological Society of America*, **76**, 803–832.

BISHOP J. K. B. and J. M. EDMOND (1976), A new large volume filtration system for the sampling of oceanic particulate matter. *Journal of Marine Research*, **34**, 181–198.

BOTTAZZI E. M., B. SCHREIBER and V. T. BOWEN (1971) Acantharia in the Atlantic: their abundance and preservation. *Limnology and Oceanography*, **16**, 677–684.

BRAMLETTE M. N. (1961) Pelagic sediments. In: *Oceanography*, M. SEARS, editor, American Association for the Advancement of Science, pp. 345–366.

BRASS G. W. and K. K. TUREKIAN (1974) Strontium distribution in GEOSECS oceanic profiles. *Earth and Planetary Science Letters*, **23**, 141–148.

BREWER P. G., G. T. F. WONG, M. P. BACON and D. W. SPENCER (1975) An oceanic calcium problem? *Earth and Planetary Science Letters*, **26**, 81–87.

BURTON W. M. and N. G. STEWART (1960) Use of long-lived natural radioactivity as an atmospheric tracer. *Nature*, **186**, 584–589.

CALVERT S. E. (1966) Accumulation of diatomaceous silica in the sediments of the Gulf of California. *Bulletin of the Geological Society of America*, **77**, 569–596.

CHUNG Y. and H. CRAIG (1973) Radium-226 in the eastern equatorial Pacific. *Earth and Planetary Science Letters*, **17**, 306–318.

COPIN-MONTEGUT C. and G. COPIN-MONTEGUT (1972) Chemical analyses of suspended particulate matter collected in the northeast Atlantic. *Deep-Sea Research*, **19**, 445–452.

CRAIG H. (1953) The geochemistry of the stable carbon isotopes. *Geochimica et Cosmochimica Acta*, **3**, 53–92.

CULMO R. (1969) Automatic microdetermination of carbon, hydrogen, and nitrogen: improved combustion train and handling techniques. *Mikrochimica acta, Wien*, 175–180.

DEGENS E. T. (1969) Biogeochemistry of stable carbon isotopes. In: *Organic geochemistry*, G. EGLINTON and M. T. J. MURPHY, editors, Springer-Verlag, pp. 304–328.

DEGENS E. T., R. R. L. GUILLARD, W. M. SACKETT and J. A. HELLEBUST (1968) Metabolic fractionation of carbon isotopes in marine plankton—I. Temperature and respiration experiments, *Deep-Sea Research*, **15**, 1–9.

DEGENS, E. T., M. BEHRENDT, B. GOTTHARDT and E. REPPMAN (1968) Metabolic fractionation of carbon isotopes in marine plankton—II. Data on samples collected off the coasts of Peru and Ecuador. *Deep-Sea Research*, **15**, 11–20.

DEUSER W. G., E. T. DEGENS and R. R. L. GUILLARD (1968) Carbon isotope relationships between plankton and seawater. *Geochimica et Cosmochimica Acta*, **32**, 657–660.

EADIE B. J. and L. M. JEFFREY (1973) ^{13}C analyses of oceanic particulate organic matter. *Marine Chemistry*, **1**, 199–209.

EDMOND J. M. (1974) On the dissolution of carbonate and silicate in the deep ocean. *Deep-Sea Research*, **21**, 455–480.

EMILIANI C. (1955) Mineralogical and chemical composition of the tests of certain pelagic Foraminifera. *Micropaleontology*, **1**, 377–380.

FEELY R. A. (1975) Major element composition of the particulate matter in the near-bottom nepheloid layer of the Gulf of Mexico. *Marine Chemistry*, **3**, 121–156.

FOWLER S. W. and L. F. SMALL (1972) Sinking rates of euphausid fecal pellets. *Limnology and Oceanography*, **17**, 293–296.

GOLDBERG E. D. and J. J. GRIFFIN (1964) Sedimentation rates and mineralogy in the South Atlantic. *Journal of Geophysical Research*, **69**, 4293–4309.

GORDON D. C., JR. (1970) A microscopic study of organic particles in the North Atlantic Ocean, *Deep-Sea Research*, **17**, 175–186.

HEEZEN B. C. and C. D. HOLLISTER (1971) *The face of the deep*, Oxford University Press, 658 pp.

HONJO S. (1975) Dissolution of suspended coccoliths in the deep-sea water column and sedimentation of coccolith ooze. In: *Dissolution of deep-sea carbonates:* W. V. SLITER, A. W. H. BÉ and W. H. BERGER, editors, Cushman Foundation for Foraminiferal Research Special Publication, **13**, 114–128.

HONJO S. (1976) Coccoliths: production, transportation and sedimentation. *Marine Micropaleontology*, **1**, 65–79.

HORIBE Y., K. ENDO and H. TSUBOTA (1974) Calcium in the South Pacific and its correlation with carbonate alkalinity. *Earth and Planetary Science Letters*, **23**, 136–140.

HUGHES M. N. (1972) *The inorganic chemistry of biological processes*, Wiley, 304 pp.

LAMBERT G. and M. NETAMI (1965) Importance des retombées seches dans le bilan du plomb 210. *Annales de geophysique*, **21**, 245–251.

LISITZIN A. P. (1972) Sedimentation in the World Ocean. *Special Publications, Society of Economic Paleontologists and Mineralogists*, **17**, 218 pp.

LURIA S. E. (1961) *The bacteria*, Academic Press, Vol. 1, pp. 1–33.

MANGELSDORF P. C., JR. and T. R. S. WILSON (1972) Constancy of ionic properties in the Pacific Ocean. *EOS, Transactions of the American Geophysical Union*, **53**, 402.

MANHEIM F. T., J. C. HATHAWAY and E. UCHUPI (1972) Suspended matter in the surface waters of the northern Gulf of Mexico. *Limnology and Oceanography*, **17**, 17–27.

MAYZAUD P. and J. L. MARTIN (1975) Some aspects of the biochemical and mineral composition of marine plankton. *Journal of Experimental Marine Biology and Ecology*, **17**, 297–310.

MCCAVE I. N. (1975) Vertical flux of particles in the ocean, *Deep-Sea Research*, **22**, 491–502.

MENZEL D. W. (1974) Primary productivity, dissolved and particulate organic matter, and the sites of oxidation of organic matter. In: *The sea*, Vol. 5, E. D. GOLDBERG, editor, Wiley, pp. 659–678.

MENZEL D. W. and R. F. VACCARO (1964) The measurement of dissolved organic and particulate carbon in seawater. *Limnology and Oceanography*, **9**, 138–142.

MOORE T. C., JR. (1969) Radiolaria: change in skeletal weight and resistance to solution. *Bulletin of the Geological Society of America*, **80**, 2103–2108.

MULLIN J. B. and J. P. RILEY (1955) The colorimetric determination of silicate with special reference to sea and natural waters. *Analytical chimica acta*, **12**, 162–176.

MURPHY J. and J. P. RILEY (1962) A modified single solution method for the determination of phosphate in natural waters. *Analytica chimica acta*, **27**, 31–36.

POET S. E., H. E. MOORE and E. A. MARTELL (1972) Lead 210, bismuth 210 and polonium 210 in the atmosphere: accurate ratio measurement and application to aerosol residence time determination. *Journal of Geophysical Research*, **77**, 5255–5265.

PORTER J. R. (1946) *Bacterial chemistry and physiology*, Wiley, 1073 pp.

REDFIELD A. C., B. H. KETCHUM and F. A. RICHARDS (1963) The influence of organisms on the composition of sea water. In: *The sea*: Vol. 2, M. N. HILL, editor, Wiley, pp. 26–77.

RILEY G. A. (1970) Particulate and organic matter in seawater. *Advances in Marine Biology*, **8**, 1–118.

ROTH P. H., M. M. MULLIN and W. H. BERGER (1975) Coccolith sedimentation by fecal pellets: laboratory experiments and field observations. *Bulletin of the Geological Society of America*, **86**, 1079–1084.

SACKETT W. M., W. R. ECKELMANN, M. L. BENDER and A. W. H. BÉ (1965) Temperature dependence of carbon isotope composition in marine plankton and sediments. *Science*, **148**, 235–237.

SACKETT W. M., B. J. EADIE and M. E. EXNER (1973) Stable isotope composition of organic carbon in recent Antarctic sediments. In: *Advances in organic chemistry, Proceedings of the 6th international meeting on organic geochemistry*, pp. 661–671.

SCHRADER H. J. (1971) Fecal pellets: role in sedimentation of pelagic diatoms. *Science*, **174**, 55–57.

SHANNON L. V., R. D. CHERRY and M. J. ORREN (1970) Polonium-210 and lead-210 in the marine environment. *Geochimica et cosmochimica acta*, **34**, 701–711.

SILKER W. B. (1972) Beryllium-7 and fission products in the GEOSECS II water column and applications of their oceanic distributions. *Earth and Planetary Science Letters*, **16**, 131–137.

SMAYDA T. J. (1971) Normal and accelerated sinking of phytoplankton in the sea. *Marine Geology*, **11**, 105–122.

SMITH K. L., JR. and J. M. TEAL (1973) Deep sea benthic community respiration: an *in situ* study at 1850 meters. *Science*, **179**, 282.

SOROKIN Y. I. (1973) Data on biological productivity of the western tropical Pacific Ocean. *Marine Biology*, **20**, 177–196.

SPENCER D. W., P. G. BREWER and M. L. BENDER (in press) The distribution of particulate Al, Ca, Sr, Ba, and Mg in the Northwestern Atlantic Ocean. *Earth and Planetary Science Letters*.

STOKES G. G. (1901) *Mathematical and physical papers*, Vol. III, Cambridge University Press, 413 pp.

STOOKEY L. L. (1970) Ferrozine—a new spectrophotometric reagent for iron. *Analytical Chemistry*, **42**, 779–781.

SVERDRUP H. U., M. W. JOHNSON and R. H. FLEMING (1942) *The oceans: their physics, chemistry and general biology*, Prentice-Hall, 1087 pp.

THOMPSON G. and V. T. BOWEN (1969) Analyses of coccolith ooze from the deep tropical Atlantic. *Journal of Marine Research*, **27**, 32–37.

TUREKIAN K. K., D. P. KHARKAR and J. THOMSON (1974) The fate of ^{210}Pb and ^{210}Po in the ocean surface, *Journal des Recherches atmospherique*, **8**, 639–646.

UN–FAO (1972) *Atlas of the living resources of the seas*, Department of Fisheries, UN–FAO, Rome.

VINOGRADOV A. P. (1953) *The elementary chemical composition of marine organisms, Memoir. Sears Foundation of Marine Research*, II, 647 pp.

WIEBE P. H., S. H. BOYD and C. WINGET (1976) Particulate matter sinking to the deep-sea floor at 2000 m in the Tongue of the Ocean, Bahamas with a description of a new sedimentation trap. *Journal of Marine Research*, **34**, 341–354.

WILLIAMS P. M. and L. I. GORDON (1970) Carbon-13: carbon-12 ratios in dissolved and particulate organic matter in the sea. *Deep-Sea Research*, **17**, 19–27.

YOUNGBLUTH M. J. (1975) The vertical distribution and diel migration of euphausids in the central waters of the eastern South Pacific. *Deep-Sea Research*, **22**, 519–536.